catalysts

MDPI

Review

Emerging Copper-Based Semiconducting Materials for Photocathodic Applications in Solar Driven Water Splitting

Mohit Kumar [1], Bhagatram Meena [1], Palyam Subramanyam [2], Duvvuri Suryakala [3] and Challapalli Subrahmanyam [1,*]

[1] Department of Chemistry, Indian Institute of Technology Hyderabad, Hyderabad 502285, Telangana, India
[2] Research Institute for Electronic Science, Hokkaido University, Sapporo 001-0020, Hokkaido, Japan
[3] Department of Chemistry, GITAM University, Visakhapatnam 530045, Andhra Pradesh, India
* Correspondence: csubbu@iith.ac.in; Tel.: +91-40-23016050

Abstract: Hydrogen production through solar-driven water splitting is a promising approach and an alternative to the conventional steam reforming of natural gas and coal gasification. The growing energy demand and environmental degradation through carbon-emitting fossil fuels urge a transition in the usage of non-renewable to renewable sources of energy. The photocathodes in a photoelectrochemical (PEC) water-splitting cell are essential for the direct evolution of hydrogen. Among the known photocathodes, Cu-based p-type semiconducting materials are the most promising photo-absorber materials owing to their low-cost, low toxicity, natural abundance, suitable bandgaps, and favorable band edges for reduction. Moreover, the chemical stability and the rate of recombination significantly limit the longevity, the PEC performance, and practical applicability of Cu-based photocathodes. To overcome these problems, it is critical to have a thorough understanding of the constraints, improvement strategies, and an assessment of current developments in order to construct and design highly stable and efficient photocathodes. Here, in this review we have summarized the development of Cu-based metal oxide and sulfide photocathodes with the significant operational challenges and strategies that have successfully been employed to enhance the PEC performance. Furthermore, the emphasis is placed on recent reports and future perspectives regarding emerging challenges.

Keywords: photocathode; H_2 production; PEC; cocatalyst; solar harvesting

Citation: Kumar, M.; Meena, B.; Subramanyam, P.; Suryakala, D.; Subrahmanyam, C. Emerging Copper-Based Semiconducting Materials for Photocathodic Applications in Solar Driven Water Splitting. *Catalysts* **2022**, *12*, 1198. https://doi.org/10.3390/catal12101198

Academic Editors: Yongpeng Liu and Yong Zuo

Received: 8 September 2022
Accepted: 7 October 2022
Published: 9 October 2022

1. Introduction

The global energy demand is rising daily, while the supply comes from the same non-renewable energy sources [1]. Carbon emissions and environmental damage are liabilities of the energy derived from fossil fuels. However, the diminishing fossil fuel sources do not provide a steady fuel supply to meet the growing population and demand. Alternative energy sources should be considered to mitigate the impact of carbon emissions and meet the energy demand. H_2 is considered a fuel for future generations with a high energy density and a lower molecular weight. At the moment, the majority of H_2 is being produced using non-renewable sources of energy processes, such as steam methane reforming, coal gasification, and coal pyrolysis. In comparison, renewable sources of H_2 production include biomass gasification & pyrolysis, thermochemical, solar-driven plasmolysis, and photoelectrolysis [2]. Presently, renewable energy sources are being scrutinized for developing reliable energy sources with no carbon emissions and a sustainable environment [3,4]. Solar energy-based technologies are attracting a vast number of applications in the form of renewable sources of energy. Solar-driven water splitting, or photoelectrochemical (PEC) water splitting, is one of the most attractive techniques used to decompose water into hydrogen (H_2) and oxygen (O_2) [5,6]. The energy falling on the earth's surface from solar radiation is a driving force for H_2 production. PEC cells use photoactive materials

coated over a transparent conductive oxide surface, mainly known as a photoanode (where oxidation of water occurs on the surface resulting in the oxygen evolution reaction OER) and photocathode (where water reduction occurs on the surface, resulting in hydrogen evolution reaction (HER)) [7,8]. The photoactive material coated films over the photoanode are generally n-type semiconductor materials and p-type semiconductor materials on the photocathode.

PEC water splitting is also known as "artificial photosynthesis." The concept of this phenomenon is nature-inspired plant leaves that convert solar light into carbohydrates. The sunlight absorbed by plant leaves is utilized by a photosystem I (PS I) and photosystem II (PS II) to generate and transfer electrons through a series of transfer processes across several redox systems, to reduce CO_2 to hydrocarbons [9]. Similarly, semiconductors, absorbing the minimum threshold wavelength of light equivalent to their bandgaps, generate photoexcited electron/hole (e^-/h^+) pairs, and the photoexcited electrons are diffused to the conduction band. Holes remain in the valence band of semiconductors, and electrons travel to the surface of the photocathode. The HER and OER occur on the surface of the photoelectrodes, and the active surface sites govern the kinetics of the reaction. The active surface sites contribute toward the adsorption of H^+ and OH− molecules on the surface of the photoelectrodes [10–12].

The seminal report on PEC water splitting, in 1972, used a thin layer of TiO_2 (E_g ~ 3.2 eV) as a photoanode for a PEC half-cell. Since then, photoanodes have been studied extensively with several material modifications and fabrication techniques. The OER takes place on the photoanode while the H_2 evolution occurs on the counter electrode [13]. The n-type semiconductors, such asTiO_2 (3.2–3.4 eV) [14], $BiVO_4$ (2.2–2.4 eV) [15], WO_3 (2.6–3 eV) [16], g-C_3N_4 (2.5–2.8 eV) [17], CdS (2.2–2.4 eV) [18], $SrTiO_3$ (3.2–3.4 eV), and Fe_2O_3 (2–2.2 eV) have been widely applied for the photoanode application in the PEC cell. Among all of these materials, TiO_2 comes out as the best material in terms of stability, while BiVO4 is the best material in abundance and light absorbing capacity in the visible region (Figure 1) [19].

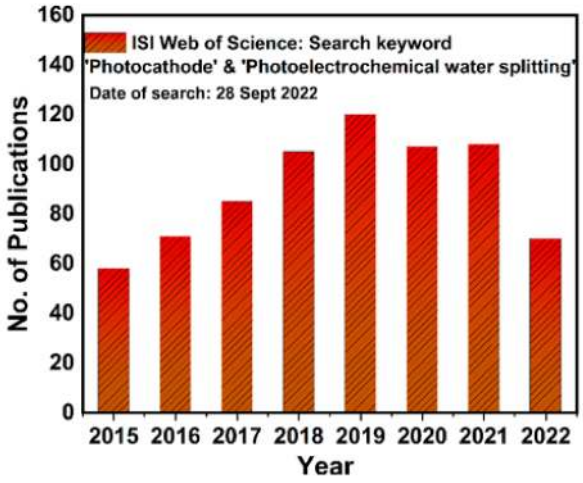

Figure 1. Year-by-year publications of photocathode research on PEC devices, the keywords were set to ("photocathode" and "photoelectrochemical water splitting"). Data are obtained from the ISI Web of Science, dated 28 September 2022.

Moreover, photocathodes have received very little attention when compared to photoanodes. Meanwhile, the direct evolution is more crucial than indirect evolution of H_2, which occurs in the photoanodic half-cells. Developing a p-type semiconductor material with a suitable bandgap, band alignment, and stability toward the oxidizing environment is paramount. Along with these physical and optical characteristics, the semiconductor must be tested for applications using non-precious and earth-abundant metals that are neither poisonous nor harmful with a sustainable approach(Figure 2) [20–24].

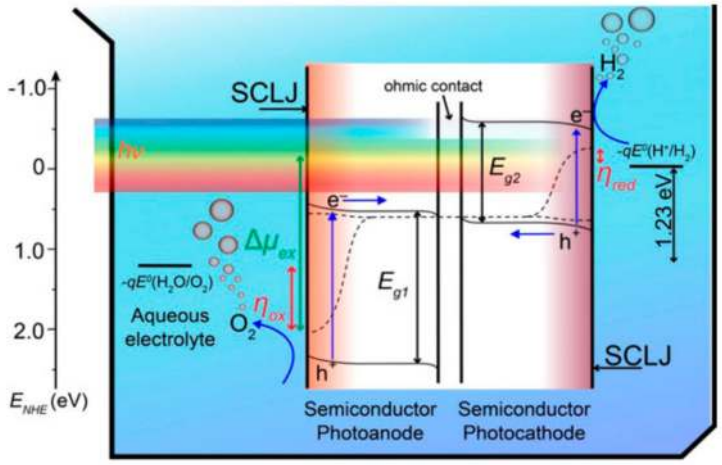

Figure 2. Schematic illustration depicting the mechanism of PEC water splitting in a tandem cell. Produced with the permission of ref. [24]. Copyright 2013, American Chemical Society.

Copper-based oxide/chalcogenide semiconductor materials are promising materials owing to their tunable band gaps, band alignment with respect to water reduction potential (Figure 3), absorption coefficients, and various synthesis procedures. In this review, we have discussed recent advancements in the synthesis and fabrication of earth-abundant copper-based oxides/chalcogenides as a functional photocathode material for solar-driven water splitting, in light of their prospective use in PEC solar-to-hydrogen systems. In addition, several modifications that took place over a period and critically assess the ongoing debates in this area, have been discussed. Finally, this evaluation provides a chance to compare Cu-based semiconductor materials to give increasing emphasis to visible light-driven solar water electrolysis.

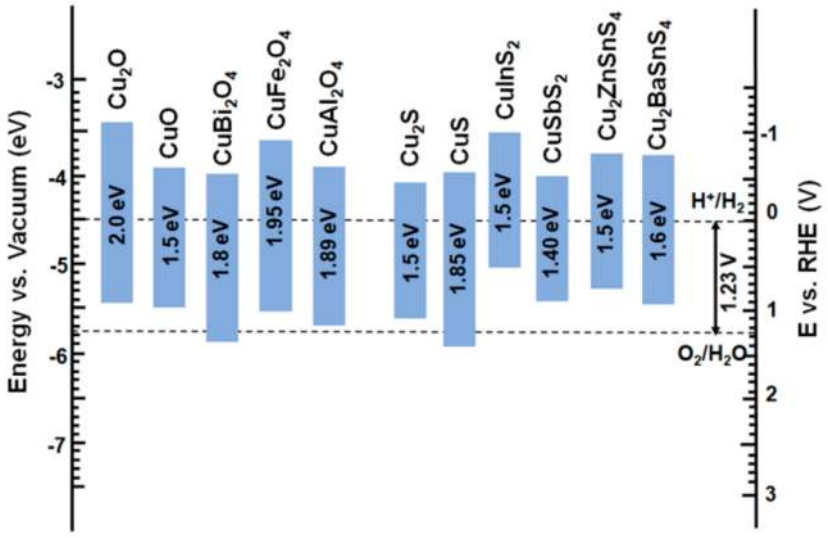

Figure 3. Energy band diagram of the various Cu-based binary, ternary, and quaternary metal oxides and sulfides.

2. PEC Water Splitting

2.1. Understanding PEC Water Splitting

PEC water splitting uses a thin semiconductor film to decompose water into hydrogen and oxygen when irradiated with adequate light energy. Photogenerated charge carriers aid the process at the semiconductor-electrolyte interface. The thermodynamics of PEC water splitting requires 285.8 kJ mol^{-1} energy, which is the same amount of energy released when hydrogen is transformed into water. The Gibbs free energy (237.2 kJ mol^{-1},

the maximum amount of energy that can be taken from the process) and the heat generated by the reaction (48.6 kJ mol^{-1}) contribute to the energy. A fuel (H_2) and an oxidant (O_2) participate as reactants in the combustion process, which is redox in nature and results in an exothermic reaction that produces water vapor. When taking into account the reverse reaction (Equation (1)), a system containing H_2O(l) may be given energy equal to Gibb's free energy (237.2 kJ mol^{-1}), which can thermodynamically transform H_2O into H_2(g) and O_2(g).

$$H_2O + 237.2\ \text{kJ mol}^{-1} + 48.6\ \text{kJ mol}^{-1} \rightarrow\ H_2(g) + \frac{1}{2}O_2(g) \quad (1)$$

The theoretical thermodynamic barrier for an overall water splitting process is proven to be 1.23 V by the fact that Gibb's free energy (237.2 kJ mol^{-1}) equates to 1.23 eV per electron. The extra heat produced by the reaction must also be considered to drive the reaction at a reasonable rate. The overpotential, or 1.48 V, is the result of converting the total energy (285.8 kJ mol^{-1}) to the potential. Traditionally, the energy needed to split water into H_2(g) and O_2(g) is known as free energy, which is equal to 237.2 kJ mol^{-1} or 1.23 V [6]. A semiconductor may theoretically generate a maximum photovoltage of 400 mV, less than the bandgap under ideal circumstances. To dissociate the water, the photoelectrode's photovoltage must be V_{ph} > 1.23 V. For PEC applications, semiconductors with a bandgap > 1.6 eV are the best options [25].

2.2. Working Principle of Water Splitting

The processes involved in the PEC water splitting process' essential operation are light absorption (step 1), charge carrier generation (step 2), charge carrier separation (step 3), and charge carrier transport to the SCLJ (step 4), where the surface reaction takes place (Figure 2). The suitable bandgap semiconductors, as previously said, absorb the light. The electron-hole pairs are excited by light absorption and subsequently separated. The electron then moves in the direction of the photocathode, leaving a hole behind. The conduction band (CB) and valence band (VB) band positions must be in the appropriate alignment for the reduction or oxidation of the water molecules in order for a semiconductor to meet the fundamental requirement. The reduction occurs on the photocathode and oxidation at the photoanode surface (Figure 2). The half-cell reactions taking place on the photoanode and photocathode are: The water-splitting reaction in the acidic electrolyte is shown in Equations (2) and (3)

$$\text{Anode}: \ 2H_2O + 4h^+ \leftrightharpoons O_2 + 4H^+ \ \Delta E^0_{OX} = 1.23\ V_{RHE} \quad (2)$$

$$\text{Cathode}: \ 4H^+ + 4e^- \leftrightharpoons 2H_2 \ \ \Delta E^0_{Red} = 0\ V_{RHE} \quad (3)$$

The water-splitting reaction in the basic electrolyte is presented in Equations (4) and (5)

$$\text{Anode}: \ 2OH^- + 4h^+ \ \leftrightharpoons O_2 + 2H_2O\ \Delta E^0_{OX} = -0.404 V_{RHE} \quad (4)$$

$$\text{Cathode}: \ 4H^+ + 4e^- \leftrightharpoons 2H_2 \ \ \Delta E^0_{Red} = -0.826\ V_{RHE} \quad (5)$$

3. Photocathode in a PEC Cell

Photocathodes are responsible for the reduction in a PEC cell serving the purpose of the direct evolution of hydrogen in a $2e^-$ transfer process over its surface. The minority charge carriers drive the reaction on the surface of the photoelectrode. To date, a number of materials have been investigated as efficient photocathodes for hydrogen generation such as p-Si (E_g = 1.1 eV) with a theoretical maximum photocurrent density -44 mA/cm^2 [26], InP (E_g = 1.3 eV) with a theoretical maximum photocurrent of -35 mA/cm^2 [27], p-GaP (E_g = 2.2 eV) [28] Sb_2Se_3 (E_g = 1.2 eV) [29], $BiSbS_3$, a p-type material with narrow bandgap (E_g = 2.2 eV)[30]. Cu-based photocathode materials have a suitable conduction band maximum for the reduction of H^+ ions and bandgap (Figure 3). The non-toxicity, earth

abundance, low-cost, high absorption coefficient, and ease of synthesis make them a promising and sustainable component for photoabsorber materials. The sluggish reaction kinetics of the HER and the recombinations require the engineering of the interfaces with the different layers which give several advantages.

4. Photocathode Materials

4.1. Cu-Based Metal Oxides for the Photocathode

Copper-based metal oxides, such as Cu_2O and CuO are among the studied metal oxides, owing to their non-toxicity, availability, nature, and bandgaps. Due to their unique optoelectronic properties, they have been extensively used in energy conversion, storage, and sensing devices. However, the chemical instability of these materials restricts their PEC performance [31]. Cu_2O has a narrow bandgap (E_g = 2.0 eV) with a theoretical photocurrent density of -14 mA/cm^2 and a 18% photoconversion efficiency (PCE) owing to its light absorption in the AM 1.5 spectrum [32]. Cu_2O, as a photocatalyst, showed a stable H_2/O_2 evolution for 1900 h in visible light ($\lambda > 460$ nm) [33]. Although Cu_2O presents an immense opportunity for the hydrogen evolution, the photodegradation and recombination rate limits its photoactive material usage. Several strategies, including surface passivation, interfacial engineering, and cocatalyst decoration, have been investigated to overcome photodegradation and suppress the recombination to fabricate efficient photocathodes [34].

Cu_2O nanowires synthesized via sputtering, anodization, and annealing sequentially showed higher J_{ph} (Figure 4a) and IPCE (Figure 4b) than planar Cu_2O. $Cu_2O/AZO/TiO_2/RuO_x$ delivered $J_{ph} = -10$ mA/cm^2 at 0 V_{RHE} and photostability beyond 55 h [35]. It is important to study the impact of pH on the photocathode and develop robust configurations for basic, neutral, and acidic mediums. The PEC activity of $Cu_2O/AZO/TiO_2/RuO_x$ was also examined at various pH levels (i.e., pH = 1, 5, and 13.6), and the deposition of the protective layer of TiO_2 played an important role in the photostability of the photocathode [36]. The deposition of NiCO-LDH over $pSi/Au/Cu_2O$ increased the photocurrent to 330% compared to $pSi/Au/Cu_2O$, due to the formation of the type-II heterojunction (Figure 4c,d), enhancing the photocarrier separation, accelerating the surface catalytic reduction reaction, and improving the stability of the $pSi/Au/Cu_2O$ photocathode [37].

A Cu_2O/CuO heterojunction photocathode modified with a Cu_2S-Pt composite exhibited an enhanced hydrogen evolution. The optimum Cu_2S and Pt used as cocatalysts deposited using SILAR and sputtering sequentially, facilitated the charge transport and suppressed recombination. $Cu_2O/CuO/Cu_2S$-9/Pt delivered J = -5.7 mA/cm^2 at 0 V_{RHE} (2.5 times of Cu_2O/CuO), while a higher onset potential (E_{op}) for $Cu_2O/CuO/Cu_2S-9/Pt$ was ~0.64 V_{RHE} observed, compared to Cu_2O/CuO (E_{op} = 0.54 V_{RHE}). The excessive Cu_2S deposition resulted in a parasitic light absorption and the creation of the recombination centers, resulting in J_{ph} fading [38].

The back contact material is essential in suppressing the recombination and charge transfer. Au is the best contact material for Cu_2O due to its large work function aligned with the valence band of Cu_2O. Recently, a CuO/NiO-based composite was investigated in place of Au using sputtering and aerial oxidation for the back contact with Cu_2O. A CuO/NiO thin film significantly improved and enhanced the transparency and hole collection (electron blocking) at the back contact of the Cu_2O photocathodes [39].

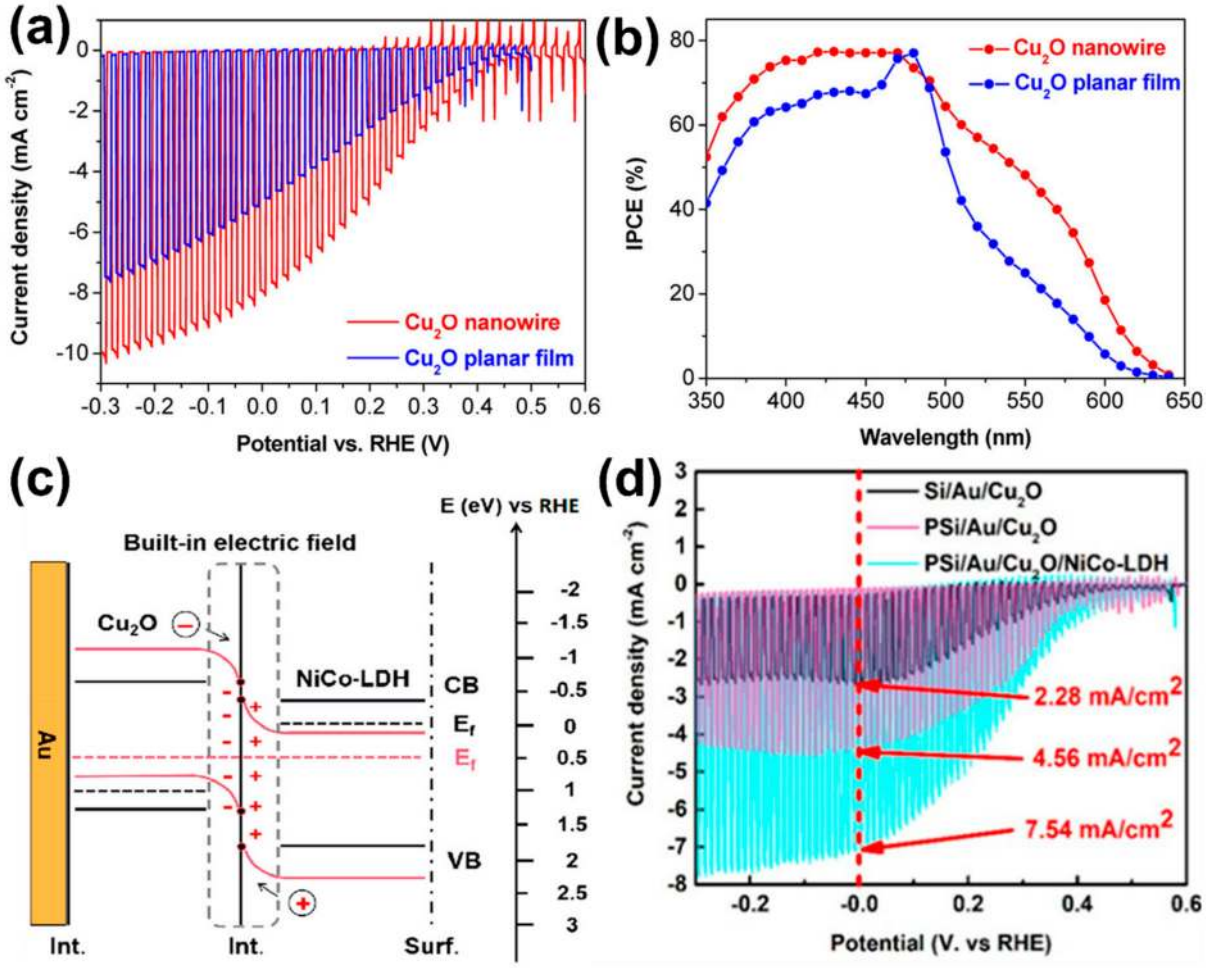

Figure 4. (**a**) J−V curves under the simulated AM 1.5G chopped illumination; (**b**) IPCE spectra under the monochromatic illumination of Cu_2O NW and planar devices. Reproduced with the permission of ref. [35]. Copyright 2016, American Chemical Society. (**c**) energy band alignment diagram of the Cu_2O/NiCo-LDH type-II heterojunction; (**d**) J–V curves of the fabricated photocathodes. Reproduced with the permission of ref. [37]. Copyright 2022, American Chemical Society.

Surface plasmon resonance (SPR), a technique that allows for the prolonged light absorption throughout the whole UV-visible spectrum of the sun, has recently been applied in the PEC water electrolysis process. SPR is a naturally occurring property of metal nanoparticles, and the collective oscillation frequency is susceptible to the size and form of the metals [40]. Photocathodes with plasmonic sandwiched metal NPs have shown great potential in boosting the PEC performance. A p-Cu_2O/AuAg/n-Cu_2O photocathode fabricated with the additional benefit of the plasmonic activity of AuAg bimetallic NPs. AuAg NPs served as a plasmonic sensitizer that increased the charge carrier concentration and, as an electron relay to boost the charge transfer between the homojunction (Figure 5a). As a result, p-Cu_2O/AuAg/n-Cu_2O achieved a higher E_{op} (~0.8 V_{RHE}) and J_{ph} when compared to the homojunction p-Cu_2O/n-Cu_2O (E_{op} = 0.7 V_{RHE}) and p-Cu_2O (E_{op} = 0.43 V_{RHE}) (Figure 5b). X-ray absorption spectroscopy (XAS) revealed the hot electron injection from plasmonic AuAg alloy to the photocathode [41].

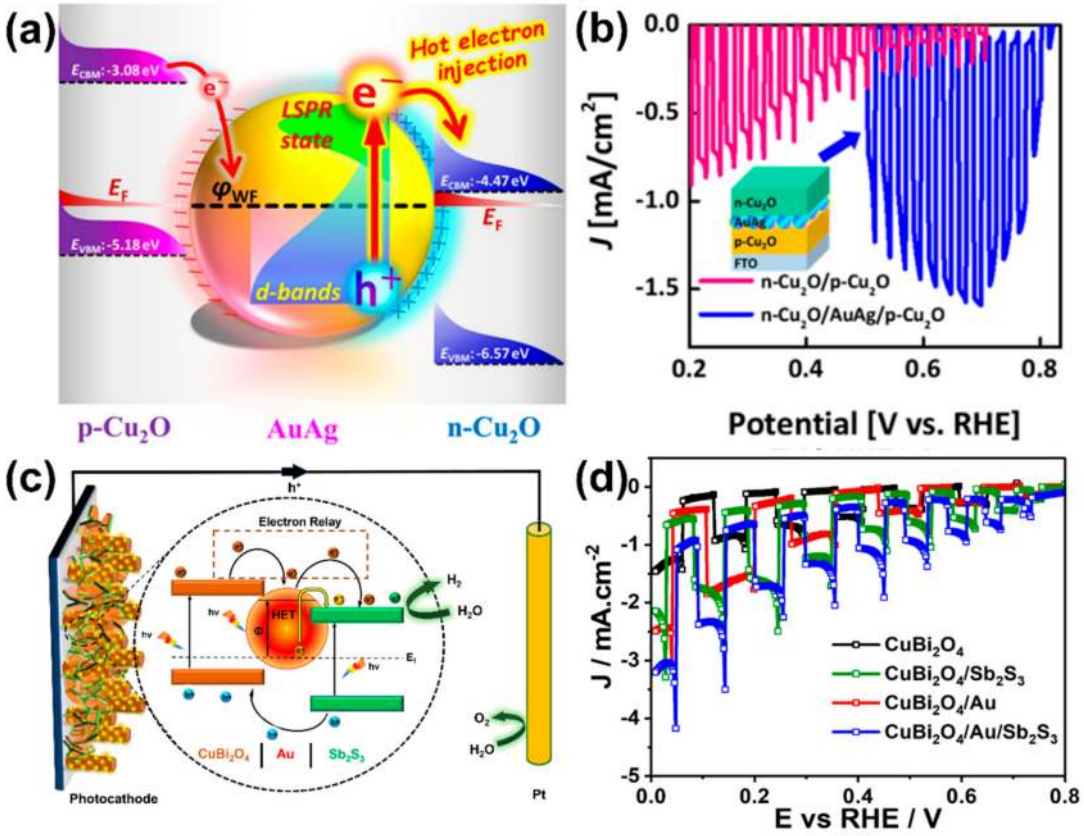

Figure 5. (**a**) Schematic Illustration of the proposed sandwich structure p-Cu_2O/AuAg/n-Cu_2O; (**b**) J–V curves of p-Cu_2O/AuAg/n-Cu_2O and p-Cu_2O/n-Cu_2O photocathodes. Produced with permission of ref. [41]. Copyright 2019, American Chemical Society. (**c**) Schematic Illustration of the charge transfer in the $CuBi_2O_4$/Au/Sb_2S_3 photocathode; (**d**) J–V curves of the $CuBi_2O_4$, $CuBi_2O_4$/Sb_2S_3 $CuBi_2O_4$/Au/Sb_2S_3 photocathode. Produced with the permission of ref. [42]. Copyright 2022, Royal Society of Chemistry.

CuO is a p-type semiconductor with a narrow bandgap (E_g = 1.3–1.7 eV) suitable for light absorption and H_2 evolution. However, the photo corrosion of CuO in the presence of light is a significant drawback for the application. The majority of J_{ph} for the CuO photocathode is due to the photo corrosion of CuO to Cu with a low faradaic efficiency of the HER (0.01%) [43]. The deposition of CdS (buffer layer) and TiO_2 (as a protective layer), and Pt as a cocatalyst sequentially resulted in an enhanced PEC performance and faradaic efficiency (~100%) [43]. Various methods have been developed to synthesize CuO having different morphologies and bandgaps. The synthesis of CuO layers using sputtering and using variable power and thickness, exhibited a different photoactivity for hydrogen evolution. The variable power of sputtering (i.e., 30, 100, 200, and 300 W) in the synthesis resulted in a different morphology of the fabricated films, while the thickness of the layer of CuO played a role in light absorption. PXRD patterns showed the poor crystallinity of CuO due to low kinetic energy for diffusion and formation of Cu-O bond, while at higher the sputtering power, good crystalline films were obtained [44]. The deposition of a protective and stable metal oxide layer has proven to improve the faradaic efficiency of the H_2 evolution. The CuO/$CuFe_2O_4$ heterostructure was fabricated using the ion impregnation method. Although the faradaic efficiency increased from 45% for the bare CuO nanowires to 100% for CuO/$CuFe_2O_4$ with an improved stability, Jph decreased to one-third of the initial J_{ph} [45]. Generating Defects in the crystal structure (e.g., copper vacancies (V_{Cu}) in CuO) is an effective way to improve the charge separation and transfer. A study showed that V_{Cu} in CuO can be tuned by changing the O_2 partial pressure in

the annealing process. The creation of vacancies in $CuBi_2O_4$ and $CuFe_2O_4$ resulted in an enhanced carrier concentration [46].

The incorporation of a foreign metal ion in the crystal structure can mitigate the issue of a photoinduced degradation. Several mixed metal oxides have been synthesized, such as $CuBi_2O_4$ [47], $CuFe_2O_4$ [48], $CuAl_2O_4$ [49], $CuNbO_3$ [50], and $CuCrO_2$ [51], and tested for the PEC photocathode application. $CuBi_2O_4$ has a bandgap of 1.5–1.8 eV and is a p-type mixed-metal oxide semiconductor that can be produced at low cost and with little environmental impact. By contributing their conduction band (CB) from the secondary metal rather than Cu 3d, ternary oxides have an advantage over the binary copper oxides in that they improve the photostability by preventing the conversion of Cu^{2+} to Cu^0. $CuBi_2O_4$ is regarded as a good photocathode material because of its advantageous narrow bandgap, band positions, low cost, visible light absorption, non-toxicity, and high flat band potential (E_{fb}) values (>1 V vs. RHE), which are advantageous for unaided solar water splitting with a small bias given by the tandem photoanode. The theoretical photocurrent density reported for $CuBi_2O_4$ under AM 1.5 G (19.5–24.5 mA/cm^2) is very far from achieved [52]. The practical photocurrent densities of the $CuBi_2O_4$ photocathodes are lower due to their poor charge transport, lower absorption coefficient, and higher charge recombination rates. Doping Ag^+ in $CuBi_2O_4$ replacing Bi^{3+} increased the hole concentration, suppressing the anodic photo corrosion [53]. The sandwiched metal NPs between the heterojunction is a new approach for different configurations of the photocathode, which have shown potential in boosting the PEC performance. The PEC performance of the N,Cu-Codoped Carbon Nanosheets/Au/$CuBi_2O_4$ photocathode was examined. Au served as a plasmonic sensitizer and electron relay to transfer the charge from $CuBi_2O_4$ to the N,Cu-Codoped Carbon nanosheets [54]. Recently, a $CuBi_2O_4$-based photocathode having Au NPs sandwiched between $CuBi_2O_4$ and Sb_2S_3 (i.e., $CuBi_2O_4/Au/Sb_2S_3$), showed an enhanced photocurrent density and PCE with respect to the bare $CuBi_2O_4$ and $CuBi_2O_4/Sb_2S_3$. Enhancement was attributed to the dual role of Au NPs: (1) plasmonic sensitizer and (2) electron relay between $CuBi_2O_4$ and Sb_2S_3 (Figure 5c). The $CuBi_2O_4/Au/Sb_2S_3$ exhibited $J_{ph} = -3.2$ mA/cm^2 which was >200% then the bare $CuBi_2O_4$ photocathode (Figure 5d) [42].

Ferrites are considered one of the best candidates, owing to their merits, including earth abundance, non-toxicity, and stability in aqueous solutions. They have narrow band gaps and suitable band positions to drive the redox reaction over their surface [55]. Copper ferrite ($CuFe_2O_4$) is a mixed metal oxide and p-type semiconductor material for the PEC photocathode with a narrow bandgap (E_g = 1.5–1.9 eV). Theoretically, it can yield a high J_{ph} (~27 mA/cm^2) and a STH efficiency (~ 33%). Although $CuFe_2O_4$ is an excellent p-type material, the crystallization temperature is high (~800–1000 °C), concerning the glass transition temperature of FTO (~564 °C). Rapid flame annealing (> 980 °C) of $CuFe_2O_4$ crystallized the film with a porous and high surface area structure which increased the light absorption (Figure 6a) and decreased the annealing time from 9 h to 16 min, when compared to conventional annealing. Changes in the bandgap and band position of CBM and VBM was observed (Figure 6b). Lesser oxygen vacancies were observed in the case of the flame-annealed $CuFe_2O_4$ films, which exhibited three times higher J_{ph} than the conventional heated $CuFe_2O_4$ (Figure 6c), and an enhanced IPCE was observed for the rapid flame-annealed $CuFe_2O_4$ films (Figure 6d) [48]. Various synthetic procedures have been reported. One is by forcibly impregnating the capped Cu^{2+} ion in a hematite (Fe_2O_3) crystal structure which resulted in drastic changes in the formation of highly porous flakes of the $CuFe_2O_4$ morphology and the crystal structure without the formation of Cu oxides. The temperature-dependent control over the degree of the spinel inversion (δ = 0.77) showed the enhanced photoelectric properties of $CuFe_2O_4$ [56]. Fabrication of the heterojunction with $CuFe_2O_4$ has been extensively examined for the enhanced charge separation. $CuFe_2O_4$/Amorphous MnO_2 (AMO) was examined for the H_2 evolution in the neutral electrolyte, and 502.8 µmol H_2 was evolved in 90 min for a 1:4 ratio of $CuFe_2O_4$/AMO, which is higher than $CuFe_2O_4/TiO_2$ (130 µmol/h) and $CuFe_2O_4$/g-C_3N_4 (76 µmol/h) [57]. Photonic crystals (PC), consisting of $CuFeO_2$ decorated microspheres

served as self-light harvesting architectures, allowing a high transmittance (~76%) and an amplified light absorption. The synthesis proceeded over the silica microspheres and the polymer-assisted synthesis. The novel design exhibited -0.2 mA/cm^2 at 0.6 V_{RHE} [58]. Various studies with Cu-based metal oxide photocathodes have been listed in Table 1.

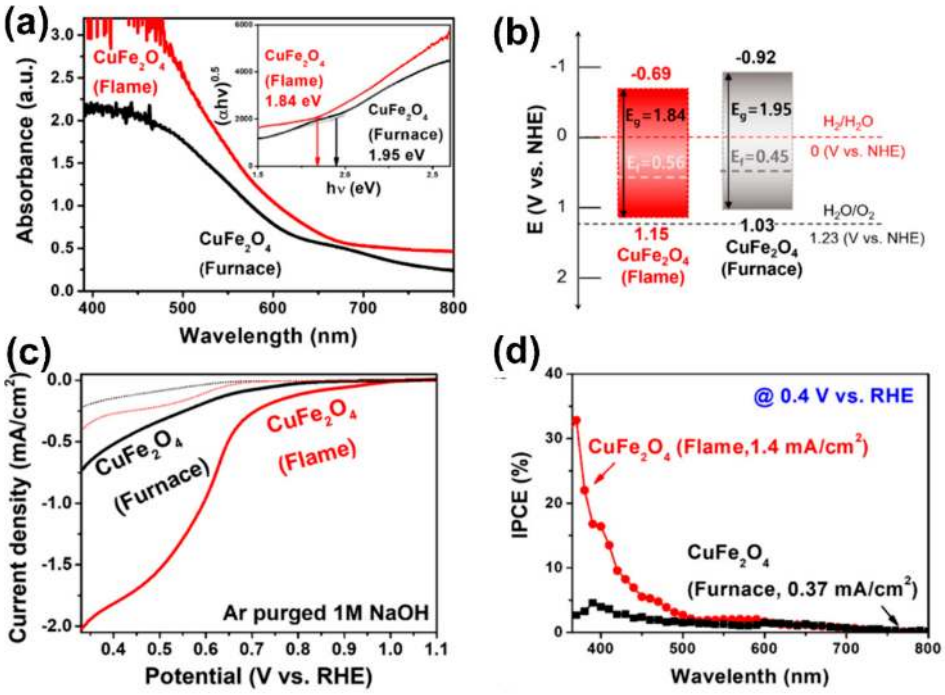

Figure 6. (**a**) UV-Vis Spectra of the rapid flame annealed and furnace annealed $CuFe_2O_4$ films; (**b**) schematic illustration band structure diagram of the flame and furnace annealed $CuFe_2O_4$ films; (**c**) J–V curves of the flame and furnace annealed $CuFe_2O_4$ films; (**d**) IPCE of the flame and furnace annealed $CuFe_2O_4$ films. Produced with the permission of ref. [48]. Copyright 2019, American Chemical Society.

4.2. Cu-Based Sulfides for Photocathode

Copper-based sulfides are promising semiconducting materials for several applications, including photovoltaics, photo-electrocatalysis, energy storage, energy conversion, sensing, CO_2 reduction, and organic degradation. Cu_2S and CuS are the most sought out of the studied materials in the recent past. Recently, copper-based ternary sulfides such as $CuInS_2$, $CuSbS_2$, $CuGaS_2$, and $CuFeS_2$, and quaternary sulfides such as $CuInGaS_2$, $Cu_2BaSnS4$, and Cu_2ZnSnS_4 have gained much attention in solar cells and PEC water splitting. Their high absorption coefficient, tunable bandgaps, optical properties, suitable band positions for a redox reaction, and tunable crystal structure make them the most prominent candidates for their application in solar harvesting. These copper-based sulfides lack photostability and crystal defects which create recombination centers. The most prominent problem is the leaching of sulfides in harsh conditions, which is the major drawback in their application in photocathodes. The scarce availability and cost aspect of In and Ga in $CuInGaS_2$ is a major drawback for its large-scale production. Researchers have developed techniques, such as the heterojunction formation, doping, metal ion substitution, creating vacancies, decoration of plasmonic metal NPs, a passivation layer, and cocatalysts to enhance the PEC performance of photoelectrodes. Engineering the surface of the photoactive material with novel robust architectures and the deposition of interlayers, such as an electron transporting layer (ETL), hole transporting layer (HTL), cocatalysts, and passivation layers which inhibit the direct contact of electrolytes with the photoactive semiconductor, is required. The deposited layers must have a good optical transparency and little to no parasitic absorption of light.

Table 1. Photoelectrochemical performances of the Cu-based metal oxide photocathodes.

Device Structure	Photocurrent (mA/cm^2); Applied Bias	Onset Potential (V_{RHE})	Stability (J/J_0); Time; Applied Bias (V_{RHE})	Maximum STH or IPCE (%)	Faradaic Efficiency	Electrolyte; Light Source	Ref.
Cu_2O/TiO_2	−0.7; −1 $V_{Ag/Agcl}$	~ 0 $V_{Ag/Agcl}$	-	-	-	0.1 M Sodium Acetate, Xe Lamp (700 mW/cm^2)	[59]
Cu_2O/Carbon	−3.95; 0 V_{RHE}	~ 0.6	~80%; 20 min; 0	0.56	-	1 M Na_2SO_4, AM 1.5G	[60]
FTO/Au/Cu_2O/AZO/TiO_2/Pt	−4.5; 0 V_{RHE}	0.4	100%;1 h; 0	0.66	-	1 M Na_2SO_4/0.1 M potassium phosphate (pH = 4.9); AM 1.5G	[61]
FTO/Au/Cu_2O/AZO/TiO_2/Pt	−6.0; 0 V_{RHE}	0.55	-	~1.5	~100%	0.5 M Na_2SO_4/0.1 M potassium phosphate (pH = 5); AM 1.5G	[62]
FTO/Au/Cu_2O/AZO/TiO_2/RuO_x	−5.0; 0 V_{RHE}	0.5	~100%; 4 h; 0	~1.1	-	0.5 M Na_2SO_4/0.1 M potassium phosphate (pH = 5); AM 1.5G	[62]
FTO/Au/Cu_2O/AZO/TiO_2/RuO_x	−5.2; 0 V_{RHE}	0.55	~100%; 25 h; 0	-	-	1 M Na_2SO_4/0.1 M potassium phosphate (pH = 4.9); AM 1.5G	[63]
FTO/Au/Cu_2O/AZO/TiO_2/MoS_x	−4.8; 0 V_{RHE}	0.45	~100%; 10 h; 0	-	100%	0.5 M Na_2SO_4/0.2 M potassium phosphate (pH = 4); AM 1.5G	[64]
FTO/Au/Cu_2O/AZO/TiO_2/Ni-Mo	−6.3; 0 V_{RHE}	0.53	~25%; 10 h; 0	-	~100%	1 M KOH (pH = 13.6); AM 1.5G	[65]
FTO/Al/Cu_2O/NiS	−5.16; 0 V_{RHE}	0.6	-	1.12	-	0.1 M Na_2SO_4; AM 1.5G	[66]
ITO/Cu/Cu_2O/TiO_2	−1.5; 0 V_{RHE}	0.55	-	0.28	98%	1 M Na_2SO_4; AM 1.5G	[67]
FTO/FeOOH/Cu_2O/Pt	−1.5; 0 V_{RHE}	0.6	66%, 1 h, 0		20%	0.1 M Na_2SO_4; AM 1.5G	[68]
FTO/Au/CuSCN/Cu_2O/Ga_2O_3/TiO_2/RuO_x	−6.4; 0 V_{RHE}	1.0	~100%; 10 h	4.2	100%	0.5 M Na_2SO_4/0.1 M NaH_2PO_4 (pH = 5); AM 1.5G	[69]
FTO/H:$Ti_3C_2T_X$/Cu_2O	−5.41; 0 V_{RHE}	0.4	-	0.55	-	1 M Na_2SO_4; AM 1.5G	[70]
Ti/Cu_2O/ZnO	−7.23; 0 V_{RHE}	0.83	-	1.77	-	0.5 M Na_2SO_4; AM 1.5G	[71]
Cu_2O/Ga_2O_3/TiO_2/RuO_x	−4.0; 0 V_{RHE}	0.8	-	60% @ 450 nm at 0 V_{RHE}	-	0.5 M Na_2SO_4/0.1 M Sodium phosphate (pH = 5); AM 1.5G	[72]
FTO/$CuBi_2O_4$/MoS_2	−0.182; 0.6 V_{RHE}	0.9	100%; 200 s; 0	-	-	0.1 M NaOH (pH = 12.5)	[73]
FTO/$CuBi_2O_4$	−0.3; 0.6 V_{RHE}	~0.8	20%; 15 min; 0.6	~14% @ 550 nm, 0.6 V_{RHE}	-	Ar-purged 0.3 M K_2SO_4/0.2 M phosphate buffer (pH = 6.65); AM 1.5G	[74]
FTO/$CuBi_2O_4$/Pt	−0.5; 0.4 V_{RHE}	~1	~10%; 3 min; 0.6	~10% @ 400 nm, 0.6 V vs. RHE	-	Ar-purged 0.3 M K_2SO_4/0.2 M phosphate buffer (pH = 6.65); AM 1.5G	[75]
FTO/CuO/$CuBi_2O_4$/Pt	−0.72; 0 V_{RHE}	-	100%; 600s; 0	-	-	0.3 M K_2SO_4/0.1 M Phosphate buffer pH = 6.8; AM 1.5G	[76]

Table 1. *Cont.*

Device Structure	Photocurrent (mA/cm^2); Applied Bias	Onset Potential (V_{RHE})	Stability (J/J_0); Time; Applied Bias (V_{RHE})	Maximum STH or IPCE (%)	Faradaic Efficiency	Electrolyte; Light Source	Ref.
$SrTiO_3/SrRuO_3/NiO/CuBi_2O_4$	−0.4 at 0 V_{RHE}	1.22	~100%; 3 h; 0	~11% @ 345 nm, 0.2 V_{RHE}~	-	0.1kPi Buffer solution (pH = 8.55); AM 1.5G	[77]
$FTO/NiO/CuBi_2O_4$	−0.5; 0.4 V_{RHE}	~1.0	~50%; 3 h; 0.4			Ar-purged 0.1 M potassium phosphate (KPi) buffered solution (pH = 8.55); AM 1.5G	[78]
FTO/CBO/ZnSe/P25	−0.43; 0.3 V_{RHE}	~1.0	~50%; 5000s; 0.3	-	-	0.3 M K_2SO_4/0.2 M phosphate buffer (pH = 6.65); 300 W Xe lamp	[79]
O_v/CBO/Zn-CBO	−0.6; 0.3 V_{RHE}	~1.0	~50%; 300s; 0.3	-	-	0.3 M K_2SO_4/0.2 M phosphate buffer (pH = 6.65); 300 W Xe lamp	[80]
FTO/Au/CBO/Pt	−1.24; 0.1 V_{RHE}	~1.0	~50%; 3000 s; 0		84.49%	0.1 M Na_2SO_4 (pH = 6.8); 300 W Xe lamp	[81]
$FTO/CuO/CuBi_2O_4$	−0.9 at 0.1 V_{RHE}	~1.0	75%; 2500 s; 0.1	0.19	-	0.5 M Na_2SO_4 solution (pH = 7); 250 W Xe lamp	[82]
$FTO/CuBi_2O_4/CdS/TiO_2/Pt$	−1; 0 V_{RHE}	~0.6	~60%; 3 h; 0	~0.13	~91%	Ar-purged 0.3 M K_2SO_4/0.2 M phosphate buffer (pH = 6.65); AM 1.5G	[83]
$FTO/CuFeO_2/AZO/TiO_2/Pt$	−1.25; 0.4 V_{RHE}	~0.9	100%; 600 s; 0.4 V_{RHE}	-	-	Ar purged 0.5 M Na_2SO_4; AM 1.5G	[84]
$FTO/CuFeO_2$/NiFe-LDH/rGO	−2.4; 0.4 V_{RHE}	~0.65	100%; 1200 s; 0.4 V_{RHE}	-	94%	1 M NaOH; AM 1.5G	[85]
$FTO/CuAlO_2/CuFeO_2$	−2.6; 0.4 V_{RHE}	~0.75	-	-	-	1 M NaOH purged with O_2	[86]

Cu_2S is a p-type material with a narrow bandgap (E_g = 1.6–2 eV) with a remarkable absorption coefficient. Cu_2S can be synthesized through various processes such as annealing, hydrothermal, hot injection method, electrodeposition, sulfurization, etc. Cu_2S nanowires arrays (NWAs) synthesized via a self-growth mechanism over the Cu foil followed by the decoration of carbon quantum dots (CQDs) remarkably enhanced the PEC performance four times that of the pristine Cu_2S NWAs [87]. Cu_xS ($0 < x \leq 1$) NPs with a copper deficiency show an inherent localized plasmonic resonance [88]. A novel solution processed ion exchange reaction to fabricate the Cu_2S films from the chemical bath deposited CdS films showed remarkable J_{ph} and PEC performances. The deposition of CdS formed a facile heterojunction with Cu_2S, TiO_2 (100 nm) served as a protective/passivation layer (Figure 7a), and RuO_x as cocatalyst. $Cu_2S/CdS/TiO_2/RuO_x$ delivered -7.0 mA/cm^2 at -0.3 V_{RHE} with E_{op} = 0.48 V_{RHE} (Figure 7b) with 90% photostability retention after 200 min [89]. MoS_2 has gained immense attention for the HER cocatalyst in recently focused research on cocatalysts. The heterojunction of $Cu_2S/MoS_2/Pt$ showed an enhanced photothermal HER performance near the NIR irradiation.

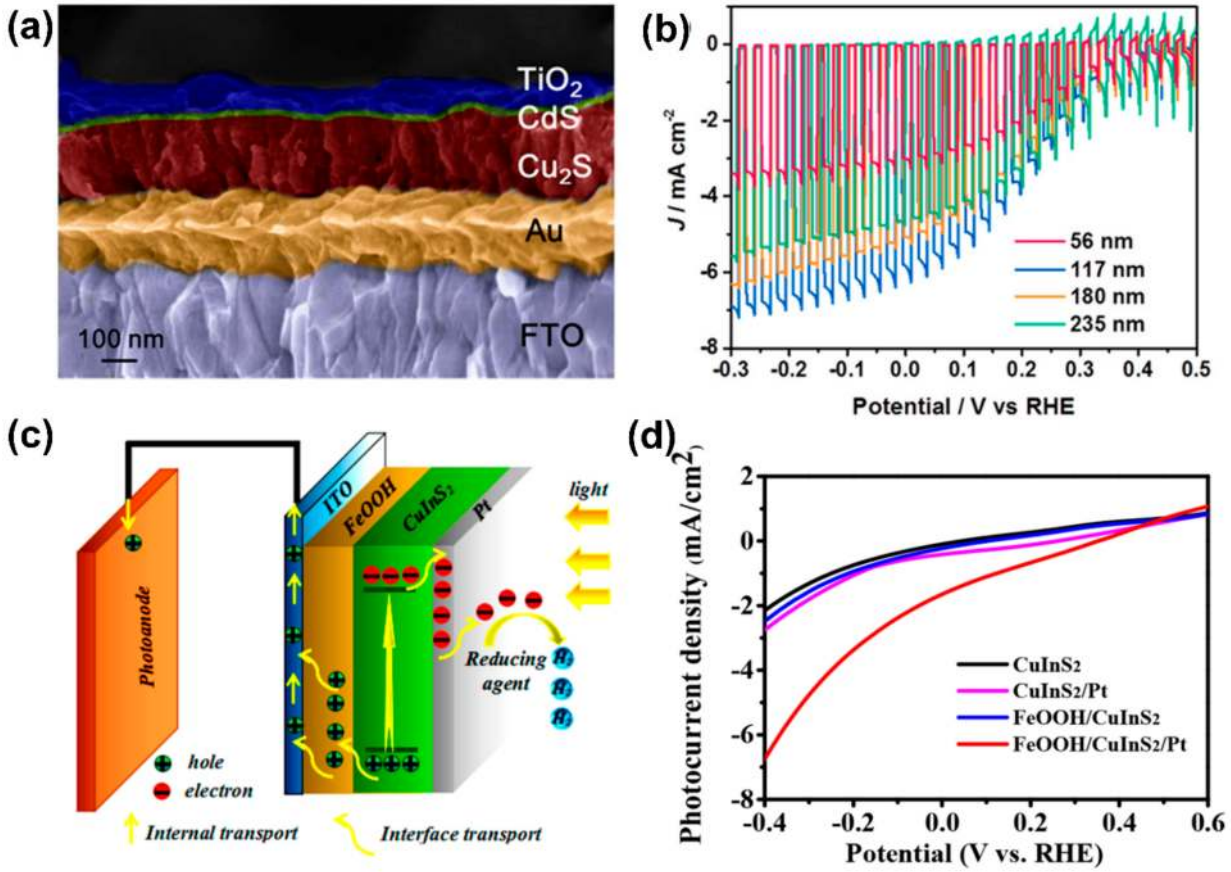

Figure 7. (**a**) Cross-sectional SEM of the different layer having FTO/Au/Cu_2S/CdS/TiO_2; (**b**) J–V curves of different thickness of the Cu_2S layer in the FTO/Au/Cu_2S/CdS/TiO_2 photocathode. Produced with the permission of ref. [89]. Copyright 2018, American Chemical Society. (**c**) Schematic illustration of the FeOOH/$CuInS_2$/Pt photocathode with an electron transfer mechanism; (**d**) J–V curves of the $CuInS_2$, $CuInS_2$/Pt, FeOOH/$CuInS_2$, FeOOH/$CuInS_2$/Pt photocathode. Produced with the permission of ref. [90]. Copyright 2018, American Chemical Society.

Ternary sulfides have an appropriate energy band structure, a wide photo-absorption range, and fast charge carrier dynamics due to the less positive valence occupied by the S 3p orbital (when compared to O 2p) and small effective mass carriers, making them promising alternatives in photovoltaic, photocatalytic, and PEC devices. For instance, altering the rate of cation exchange or the proportion of the sulfur precursor during the synthesis process,

may be used to create ternary Cu-In-S materials with various crystal morphologies, compositions, and switchable n-type and p-type semiconducting characteristics [91]. $CuInS_2$ (E_g ~ 1.5–1.8 eV) is a photoactive material in solar cells and PEC photocathodes. Along with the merits, $CuInS_2$ suffers from a high rate of recombination. Therefore, the $CuInS_2$-based photocathodes have been modified with other materials to improve PCE. Fabrication of the heterojunction generates an inbuilt electric field that helps in the charge separation and the enhanced light absorption.

The deposition of a hole transporting layer below the $CuInS_2$ layer helps in the charge separation and inhibits the recombination in the photoexcited charge carriers. FeOOH/$CuInS_2$/Pt was fabricated with FeOOH as a hole transporting layer, selectively (Figure 7c). FeOOH/$CuInS_2$/Pt delivered $J_{ph} = -6$ mA/cm^2 at -0.4 V_{RHE} (Figure 7d) [90]. In another study, a NiO/$CuInS_2$/NiS photocathode was fabricated where NiO served as hole transporting layer while NiS served as a cocatalyst and passivation layer [92]. The investigation of a facile heterojunction formation using CdS and In_2S_3 with $CuInS_2$ was studied by fabricating $CuInS_2$/CdS/Pt and $CuInS_2$/In_2S_3/Pt. The $CuInS_2$/In_2S_3/Pt photocathode delivered a higher STH efficiency (~ 2.9%), while $CuInS_2$/CdS/Pt delivered (~1.8%). XPS revealed the notch-type positive conduction band offset with In_2S_3/$CuInS_2$, while CdS/$CuInS_2$ formed an unfavorable negative cliff type negative offset [93]. Recently, the charge transfer and photoelectrochemical activity of the $CuInS_2$-based photoelectrodes have been improved by an atomic gradient passivation layer $(Ta, Mo)_x$ $(O, S)_y$ [94]. A metal ion substitution is another approach that improves the optical properties and modulates the crystal structure, changing the material's bandgap, open circuit potential (OCP), and photostability in a PEC cell [95,96]. The Ga substitution with In in a $CuInS_2$ crystal structure has shown an enhanced PEC performance. Different Ga/(Ga + In) ratios (0, 0.10, 0.25, and 0.40) were synthesized with respect to $CuInS_2$. E_g increased with the amount of Ga (1.52, 1.58, 1.67, 1.80 eV), respectively. CBM and VBM were observed to change, which aided the enhanced light absorption and the OCP. Pt-CdS/CIGS(25) corresponding to the Ga/(Ga + In) ratio (0.25) exhibited 6.78 mA/cm^2 at 0 V_{RHE} in 0.1 M Na_2SO_4 (pH 9) and a higher $E_{op} = 0.89$ V_{RHE}, as compared to other ratios [97]. The Ag substitution in $CuGaS_2$ fabricating $Cu_{1-x}Ag_xGaS_2$ (x = 0–1.0) and the insertion of Ag in the crystal structure was observed with a change in VBM [98].

Recently, $CuSbS_2$ has gained attention in the PEC photocathodic approach. It has also been used as HTL in solar cells for the hole extraction [99,100]. Synthetic procedures include thermal evaporation [101,102], electrodeposition [103], sputtering [104], CBD [101], pyrolysis [105], etc. In a recent study, $CuSbS_2$ exhibited a temperature-dependent bandgap (E_g = 1.57–1.58 eV). A $CuSbS_2$/Sb_2Se_3/TiO_x/Pt photocathode was fabricated which exhibited a remarkable $J_{ph} = -18$ mA/cm^2 at 0 V_{RHE} in 1 M H_2SO_4. The $CuSbS_2$ film acted as a hole transporting layer and a photoactive material, suppressing the recombination rate. In another study, the facile heterojunction of $CuSbS_2$ with CdS was synthesized and examined for the PEC photocathode. $CuSbS_2$/CdS/Pt delivered $J_{ph} = -4.1$ mA/cm^2 at 0 V_{RHE} and $E_{op} = 0.45$ V_{RHE} [106].

Quaternary copper-based sulfides are the newly emerging most interesting p-type materials (e.g., Cu_2ZnSnS_4) with the promising potential for solar harvesting applications. Synthesis procedures involved in the fabrication of films are hydrothermal, molecular ink, electrodeposition, and vacuum-based synthesis. The rapid progress in materials to achieve the target efficiency of these sulfides are hindered by the narrow phase stability of the quaternary phase and the existence of secondary phases, such as ZnS, Cu_2S, SnS, SnS_2, and Cu_2SnS_3, and to defects leading to poor performance and repeatability [107]. In early reports, Mo/Cu_2ZnSnS_4/CdS/AZO/TiO_2/Pt was fabricated via electrodeposition (sequential and simultaneous). Moreover, the examined photocathode showed over -1 mA/cm^2 at 0 V_{RHE} in the simultaneous electrodeposition [108]. The buffer layer formed over Cu_2ZnSnS_4 was scrutinized with CdS and In_2S_3, and the Cu_2ZnSnS_4/CdS/In_2S_3/Pt fabricated showed a higher J_{ph} and PCE, as compared to Cu_2ZnSnS_4/CdS/Pt. The modification with an In_2S_3/CdS double layer followed by the deposition of Pt exhibited STH

(%) ~ 1.63% [109]. A HfO_2 layer was particularly effective at surface passivating the CdS/Cu_2ZnSnS_4 photocathode, which increased the photoelectrochemical stability. With a 6 nm thick HfO_2 layer added, the CdS/Cu_2ZnSnS_4 photocathode demonstrated a long-term photocurrent stability of over 10 h while maintaining a high half-cell solar-to-hydrogen efficiency (HC-STH) of 2.7% at 0.36 V_{RHE}. A full PEC cell was fabricated using a $BiVO_4$-based photoanode [110]. The molecular ink-derived Cu_2ZnSnS_4 (CZTS) films were synthesized via spin coating. The study showed the sequence of the precursor addition in the 2-methoxyethanol (2-ME) and the films synthesized with the configuration CZTS/CdS/ALD-TiO_2/Pt. CdS served as a buffer layer, TiO_2 as a passivation layer, and Pt coated as a cocatalyst for the HER. CZTS/CdS/ALD-TiO_2/Pt delivered -21.5 mA/cm^2 at -0.2 V_{RHE} with a 40–45% faradaic efficiency, showing side reactions as the surface of CZTS is not fully covered [111].

The metal ion substitution has been studied and proved to improve the optical properties of Cu_2ZnSnS_4. The substitution of Cu with Ag and Zn with X (X = In^{+3}, Cd^{+2}, Sb^{+3}, Bi^{+3}) have been studied extensively with the application in the PEC cells and solar cells. The photocurrent produced by a $Cu_2Cd_{0.4}Zn_{0.6}SnS_4$ (CCZTS) photoabsorber coated with CdS/TiMo/Pt is claimed to be -17 mA/cm^2 at 0 V_{RHE}, which is at least three times larger than the photocurrent produced by a pure Cu_2ZnSnS_4. The XPS studies revealed a 0.13 eV spike-like offset when integrated with CdS, which enhanced the charge separation and transfer [112]. A low Ag substitution in Cu_2ZnSnS_4 revealed an enhanced J_{ph} and E_{op}. Cu^+ was partially substituted with Ag^+ ion in the $(Ag_xCu_{1-x})_2ZnSnS_4$ (x-ACZTS) (x = 0.04, 0.08, 0.10) crystal structure synthesized via a molecular ink precursor spin-coated over the transparent conductive oxide. In comparison to the CZTS/CdS/Pt photocathode, which has a photocurrent of -13 mA/cm^2 and an onset potential of 0.65 V_{RHE}, the ACZTS/CdS/Pt photocathode produces a maximum photocurrent of -17.7 mA/cm^2 at 0 V_{RHE} with 4% Ag (x = 0.04) and a maximum onset potential of 0.85 V_{RHE} with 8% Ag (x = 0.08) [113].

Another new class of materials when Zn is replaced with Ba in CZTS is an earth-abundant emerging material for PV applications [114]. Cu_2BaSnS_4 is a p-type material (E_g ~ 1.5–2.0 eV) with a readily available and cost-effective material that can be synthesized on a large scale. The maximum theoretical maximum J_{ph} obtained is -14 mA/cm^2, according to the Schokley–Queisser limit (Q–S limit) [115]. At a high temperature, CBTS decomposes to Cu_4BaS_3 and $Cu_2Ba_3Sn_2S_8$ (E_g = 2.19 eV) in the presence of a low partial pressure of sulfur [116]. Large grain Cu_2BaSnS_4 (CBTS) films were synthesized using a green synthetic approach using polyethyleneimine and EDA. The Mo/CBTS (260 nm) photocathode exhibited $J_{ph} = -4$ mA/cm^2 at 0 V_{RHE} in 0.1 M Na_2SO_4 (pH = 7) with no degradation of J_{ph} up to 2 h. With a remarkable charge carrier concentration of 1.8×10^{21} cm^{-3}, the charge carrier mobility in the large grains was 1.29 cm^2/V·s [117]. In another study, CBTS/CdS/ZnO/TiO_2 was fabricated using co-sputtering Cu, SnS, and BaS on the target FTO (Figure 8a,b). The CdS shows a smaller lattice mismatch with CBTS, while ZnO and TiO_2 CBM are aligned so that the facile electron transfer can occur for the surface reduction. CBTS/CdS/ZnO/TiO_2 showed a higher J_{ph} (-7.8 mA/cm^2 at -0.1 V_{RHE}) and IPCE (%) in the neutral electrolyte, as compared to the bare CBTS (-4.8 mA/cm^2 at -0.2 V_{RHE}) (Figure 8c,d) [118]. The substitution of S with Se forming CBTSSe is another effective way to improve the crystal structure and electronic properties of the CBTS. $Cu_2BaSnS_{4-x}Se_x$ (x = 3) (CBTSSe) was synthesized by co-sputtering followed by sulfurization. The CBTSSe (x = 3)/CdS/TiO_2/Pt photocathode was fabricated using a chemical bath deposition for CdS followed by ALD for TiO_2 and the electrodeposited Pt. The resulting photocathode showed -12 mA/cm^2 at 0 V_{RHE} with STH (%) 1.09% with a remarkable stability up to 10 h [119]. CBTSSe (x = 3) was powder synthesized via ball milling, and a photocathode with the configuration Mo/CBTSSe (x = 3)/CdS/TiO_2/Pt exhibited a photocurrent of -4.69 mA/cm^2 at 0 V_{RHE} with STH (%) 0.49%. The synthetic procedures also affect the STH (%) of the photocathode with the solution based CBTSSe (0.89%), vacuum-based (1.09%) and ball milling (0.49%) [120]. Various studies with Cu-based metal sulfides photocathodes have been listed in Table 2.

Table 2. Photoelectrochemical performances of the Cu-based metal sulfide photocathodes.

Device Structure	Photocurrent (mA/cm^2); Applied Bias	Onset Potential (V_{RHE})	Stability (J/J_0); Time; Applied Bias (V_{RHE})	Maximum STH or IPCE (%)	Faradaic Efficiency	Electrolyte; Light Source	Ref.
FTO/Au/Cu_2S/CdS/TiO_2/RuO_x	−2.5; −0.3 V_{RHE}	0.42	76%; 12 h; 0	-	-	1 M kPi buffer solution (pH = 7); AM 1.5G	[121]
FTO/Cu_2S/Cu_2O/Cu foam Au/Cu_2S/CdS/TiO_2/RuO_x	−5.05; 0 V_{RHE}	0.35	80%; 1 h ; 0	40% @ 450 nm at 0 V_{RHE}	-	1 M Na_2SO_4/0.1 M KH_2PO_4 at (pH 4.9); AM 1.5G	[122]
FTO/Cu_2O/Cu_2S	−4.1; −0.6 $V_{Ag/AgCl}$	−0.29 $V_{Ag/AgCl}$	-	0.38	-	0.5 M Na_2SO_4; AM 1.5G	[123]
FTO/Cu_2O/Cu_2S-Ni	−1.70; 0 V_{RHE}	0.5	45%; 500 s; 0	-	-	0.5 M Na_2SO_4; 300 W Xe lamp with AM 1.5G filter	[124]
FTO/$CuInS_2$/CdS@MBAs	−0.487; −0.15 V_{RHE}	-	~100%; 400 s; 0	10% @ 400 nm at 0 V_{RHE}	-	1 M KCl Solution (pH = 5.97); AM 1.5G	[125]
FTO/$CuInS_2$/Sb_2S_3/Pt	−2.48; −0.6 V_{RHE}	0.6	~88%; 180 s; −0.6	21.41% @ 550 nm at −0.6 V_{RHE}	-	0.1 M Na_2SO_4 (pH = 7.1); AM 1.5G	[126]
FTO/$CuInS_2$/CdS	−0.71; −0.2 V_{RHE}	0.25	~100%; 1500 s; 0	9% @ 425 nm at 0 V_{RHE}	-	1 M KCl Solution (pH = 5.97); 500 W Xe lamp with AM 1.5G filter	[127]
Mo/$CuInS_2$/In_2S_3/Pt	−5.6; 0 V_{RHE}	0.7	~100%;80 min; 0.1	0.7	100%	0.1 M Na_2SO_4 (pH = 10); AM 1.5G	[128]
FTO/$CuInS_2$/CdS/AZO/TiO_2/Pt	−3.5; −0.3 V_{RHE}	0.6	80%; 2 h; 0	~20% @ 500 nm at 0 V_{RHE}	-	0.5 M Na_2SO_4/0.1 M KH_2PO_4 (pH = 5.0); 300 W Xe lamp with AM 1.5G filter	[129]
FTO/CIS NR/CdS/ZnS	−2.0; 0.3 V_{RHE}	1.06	~100%; 3000 h; 0.3	-	-	0.5 M Na_2SO_4 (adjusted to pH 10 by adding NaOH).; AM 1.5G	[130]
FTO/$CuInS_2$/SnS_2-1.6/C_{60}	−4.51; −0.45 V_{RHE}	-	-	8% @ 450 nm at −0.45 V_{RHE}	-	0.5 M Na_2SO_4; AM 1.5 G	[131]
FTO/Au-$CuInS_2$	−15.2; 0 V_{RHE}	0.3 V_{SCE}	~100%; 400 s; −0.5 V_{SCE}	4.29	-	0.5 M Na_2SO_4; AM 1.5G	[132]
FTO/$CuSbS_2$/Sb_2Se_3/TiO_2/Pt	−18.0; 0 V_{RHE}	0.2	-	-	-	1 M H_2SO_4 (pH = 0); AM 1.5G	[133]
FTO/CZTS/CdS/TiO_2-Pt	−9.0; 0 V_{RHE}	0.6	-	1.2	-	0.1 M Na_2SO_4 (pH = 9.5); 300 Xe lamp with AM 1.5G filter	[134]
FTO/CZTS/CdS/ZnO/Pt	−8.0; 0 V_{RHE}	0.63	~100%; 2 h; 0	2.1	-	0.2 M Na_2HPO_4/NaH_2PO_4 (pH 6.5); 300 W Xe lamp with AM 1.5G filter	[135]
FTO/CZTS/HfO_2/CdS/HfO_2/Pt	−28.0; 0 V_{RHE}	0.7	~100%; 24 h; 0	2.4	-	0.2 M Na_2HPO_4/NaH_2PO_4 (pH 6.5); AM 1.5G filter	[136]
FTO/ACZTS/CdS/Pt	−3.78; 0 V_{RHE}	0.33	~100%; 1 h; 0	0.32	95%	0.2 M Na_2HPO_4 (pH = 10); AM 1.5G	[137]
FTO/ACZTS/CdS/In_2S_3/Pt	−15.0; 0 V_{RHE}	0.7	~50%; 3 h; 0	2.4	98%	0.2 M K_2HPO_4/KH_2PO_4 (pH = 6.85); AM 1.5G	[138]
FTO/CGZTS/CdS/In_2S_3/Pt	−11.1;	0.6	90%; 7000 s; 0	1.7	-	0.2 M K_2HPO_4/KH_2PO_4 (pH = 6.85); AM 1.5G	[139]

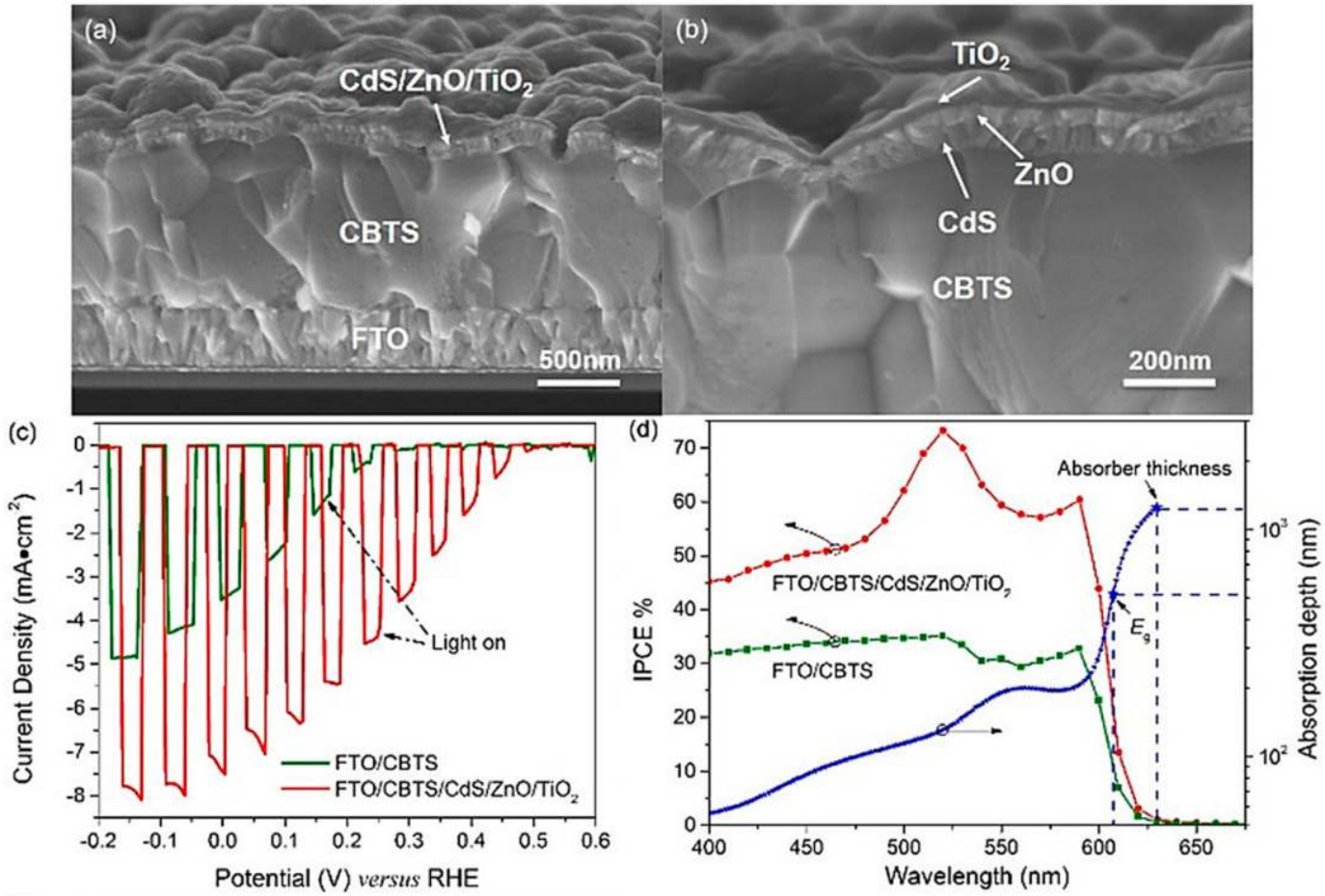

Figure 8. (**a**) Cross-sectional SEM image of the FTO/CBTS/CdS/ZnO/TiO_2 photocathode; (**b**) magnified cross-sectional SEM image showing the structural detail at the interface of CBTS/CdS/ZnO/TiO_2; (**c**) J–V curves of FTO/CBTS and FTO/CBTS/CdS/ZnO/TiO_2; (**d**) IPCE spectra measured at the potential of 0 V versus RHE and the absorption depth ($1/\alpha$) of CBTS. Produced with the permission of ref. [118]. Copyright 2016, American Chemical Society.

5. Conclusions

PEC water splitting, a promising method to generate hydrogen using renewable solar energy, still suffers from issues such as photostability, longevity, efficiency, recombination, and side reactions. The development of robust and energy-efficient photoabsorber films is of prime importance, along with the overall efficiency of PEC cells. Cu-based metal oxides/sulfides are cost-effective, earth-abundant, and prime candidates as p-type semiconductors in photocathodes. In this review, the latest Cu-based photocathodes for PEC water splitting have been outlined, along with the different photocathode materials modifications and the operational challenges associated with the visible-light-driven water splitting. In theory, the reduction potentials of water must be overlapped by the band gap energy levels for the water splitting to occur independently, and as a result, the photoinduced charge carriers must have the proper overpotential for the HER. Notably, the semiconductor must have an excellent absorption coefficient, and the Cu-based semiconductors constitute all of the currently used materials' inexpensive and scalable photocathode semiconductors. Although they have not yet reached the theoretical maximum photocurrent, they are unstable because of the material degradation. It is critical to identify the source of the instability. The chemical stability at the surface of the photoelectrodes should be examined in great detail, and the surface of the photocathodes should be provided with photostable layers that can withstand harsh conditions. Using stable interlayers should avoid the direct

contact of the layers with electrolytes that are unstable under light illumination conditions. The interlayers with a low parasitic light absorption that can act as a selective charge transporting layers must be investigated. To balance the light absorption and the parasitic light absorption, the thickness optimization of these interlayers, a passivation layer, and a photoabsorber layer with an excellent transparency will be an intriguing challenge.

Numerous primary and complex synthetic techniques for the Cu-based binary metal oxides with morphological control are known. Even though these oxides have a remarkable PEC conversion efficiency, their photostability is relatively poor. Meanwhile, ternary metal oxides are more resistant to photo corrosion than binary oxides, although their photocurrents obtained are by far pretty minimal, compared to the theoretical maximum photocurrent. Furthermore, these ternary oxides suffer from strong recombinations, leading to poor a PEC performance. The likelihood of the crystal structural alterations is more likely in the ternary metal oxides than in the binary metal oxides, which might be helpful in numerous ways, including increasing the photostabilities and reducing the recombinations. While the Cu-based metal sulfides are good light absorbers, sulfur leaching in the presence of light during the water splitting is a concern for photoactive material deterioration. However, ternary and quaternary metal sulfides have demonstrated a higher activity and the PEC efficiency than oxides. They fail the longevity tests for their application. The multi-step PEC water splitting process begins with a charge carrier generation, separation, and migration, which are crucial aspects regulating the fate of a specific PEC efficiency. The recombinations in the semiconductor layer restrict the charge production by the photoexcitation of the semiconductors. The Cu-based metal oxide/sulfides may be manufactured using novel manufacturing procedures to achieve longer diffusion lengths and lower recombination rates. Due to the striking improvement in the crystal structure, the electrical characteristics, and the photocurrent density in the PEC cells, the cation substitution in the Cu-based sulfides, such as CIGS, CZTS, CBTS, etc., has attracted enormous attention. Currently, the ions used in the replacements are either hazardous or costly. Earth-abundant, non-toxic cations must be investigated for the cation substitution in the crystal structure replacement. A novel synthesis and layer loading strategies over the photoactive layer must be investigated to provide the effective interaction between the layers for the efficient charge transfer and to minimize the charge transfer resistance.

The main concerns of photostability and the PEC efficiency can be overcome by engineering the interfaces in photoelectrode. Using electron transporting layers (ETLs) and hole transporting layers (HTLs), along with stable buffer layers to form efficient heterojunctions can be fruitful in developing a robust photoelectrode. The decoration of an optically transparent cocatalyst that can serve as a passivation layer and boost the kinetics of the surface reactions would be of great potential. The cocatalyst layer deposition can be advantageous in minimizing the side reactions and enhancing the faradaic efficiency. The study of the interaction between different layers, including the semiconductor layer and the cocatalyst with different rational configurations, such as core-shell structures and 3D porous structures with a minimum mismatch in the crystal lattice, energy levels, and electronic structure. In order to allow for an adequate light absorption and charge separation, semiconductor photocathodes must control their shape and semiconducting nature.

The development of highly active photocathode materials will continue, and it will not be long until a confident band gap design becomes a norm.

Author Contributions: Contribution statement for the authors of CRediT. The first author is M.K.: Conceptualization, Investigation, Visualization, Writing Original draft, B.M.: Data curation, Methodology, Writing Original draft, Software. P.S.: Validation, Investigation, Data Curation. D.S. Validation, Investigation, Data Curation. The corresponding author, C.S.: Conceptualization, Investigation, Visualization, Supervision, Validation, Writing Original draft. All authors have read and agreed to the published version of the manuscript.

Funding: This research received no external funding.

Acknowledgments: Mohit Kumar and Bhagatram Meena would like to thank CSIR-India for the fellowship. Authors would like to thank the JICA for the financial support under the JICA-IITH Friendship 2.0.

Conflicts of Interest: The authors declare no conflict of interest.

References

1. Waheed, R.; Sarwar, S.; Wei, C. The Survey of Economic Growth, Energy Consumption and Carbon Emission. *Energy Rep.* **2019**, *5*, 1103–1115. [CrossRef]
2. Younas, M.; Shafique, S.; Hafeez, A.; Javed, F.; Rehman, F. An Overview of Hydrogen Production: Current Status, Potential, and Challenges. *Fuel* **2022**, *316*, 123317. [CrossRef]
3. Staffell, I.; Scamman, D.; Abad, A.V.; Balcombe, P.; Dodds, P.E.; Ekins, P.; Shah, N.; Ward, K.R. The Role of Hydrogen and Fuel Cells in the Global Energy System. *Energy Environ. Sci.* **2019**, *12*, 463–491. [CrossRef]
4. Sharif, A.; Raza, S.A.; Ozturk, I.; Afshan, S. The Dynamic Relationship of Renewable and Nonrenewable Energy Consumption with Carbon Emission: A Global Study with the Application of Heterogeneous Panel Estimations. *Renew. Energy* **2019**, *133*, 685–691. [CrossRef]
5. Jacobsson, T.J. Photoelectrochemical Water Splitting: An Idea Heading towards Obsolescence? *Energy Environ. Sci.* **2018**, *11*, 1977–1979. [CrossRef]
6. Walter, M.G.; Warren, E.L.; McKone, J.R.; Boettcher, S.W.; Mi, Q.; Santori, E.A.; Lewis, N.S. Solar Water Splitting Cells. *Chem. Rev.* **2010**, *110*, 6446–6473. [CrossRef]
7. Sivula, K.; van de Krol, R. Semiconducting Materials for Photoelectrochemical Energy Conversion. *Nat. Rev. Mater.* **2016**, *1*, 15010. [CrossRef]
8. Hisatomi, T.; Kubota, J.; Domen, K. Recent Advances in Semiconductors for Photocatalytic and Photoelectrochemical Water Splitting. *Chem. Soc. Rev.* **2014**, *43*, 7520–7535. [CrossRef]
9. Whang, D.R.; Apaydin, D.H. Artificial Photosynthesis: Learning from Nature. *ChemPhotoChem* **2018**, *2*, 148–160. [CrossRef]
10. Yang, Y.; Niu, S.; Han, D.; Liu, T.; Wang, G.; Li, Y. Progress in Developing Metal Oxide Nanomaterials for Photoelectrochemical Water Splitting. *Adv. Energy Mater.* **2017**, *7*, 1–26. [CrossRef]
11. Chaves, A.; Azadani, J.G.; Alsalman, H.; da Costa, D.R.; Frisenda, R.; Chaves, A.J.; Song, S.H.; Kim, Y.D.; He, D.; Zhou, J.; et al. Bandgap Engineering of Two-Dimensional Semiconductor Materials. *NPJ 2D Mater. Appl.* **2020**, *4*, 29. [CrossRef]
12. Su, J.; Vayssieres, L. A Place in the Sun for Artificial Photosynthesis? *ACS Energy Lett.* **2016**, *1*, 121–135. [CrossRef]
13. Fujishima, A.; Honda, K. Electrochemical Photolysis of Water at a Semiconductor Electrode. *Nature* **1972**, *238*, 37–38. [CrossRef]
14. Subramanyam, P.; Kumar, P.N.; Deepa, M.; Subrahmanyam, C.; Ghosal, P. Bismuth Sulfide Nanocrystals and Gold Nanorods Increase the Photovoltaic Response of a TiO_2/CdS Based Cell. *Sol. Energy Mater. Sol. Cells* **2017**, *159*, 296–306. [CrossRef]
15. Subramanyam, P.; Vinodkumar, T.; Nepak, D.; Deepa, M.; Subrahmanyam, C. Mo-Doped $BiVO_4$@reduced Graphene Oxide Composite as an Efficient Photoanode for Photoelectrochemical Water Splitting. *Catal. Today* **2019**, *325*, 73–80. [CrossRef]
16. Subramanyam, P.; Meena, B.; Sinha, G.N.; Deepa, M.; Subrahmanyam, C. Decoration of Plasmonic Cu Nanoparticles on WO_3/Bi_2S_3 QDs Heterojunction for Enhanced Photoelectrochemical Water Splitting. *Int. J. Hydrogen Energy* **2020**, *45*, 7706–7715. [CrossRef]
17. Subramanyam, P.; Meena, B.; Suryakala, D.; Deepa, M.; Subrahmanyam, C. Plasmonic Nanometal Decorated Photoanodes for Efficient Photoelectrochemical Water Splitting. *Catal. Today* **2020**, *379*, 1–6. [CrossRef]
18. Li, J.; Cushing, S.K.; Zheng, P.; Senty, T.; Meng, F.; Bristow, A.D.; Manivannan, A.; Wu, N. Solar Hydrogen Generation by a CdS-Au-TiO_2 Sandwich Nanorod Array Enhanced with Au Nanoparticle as Electron Relay and Plasmonic Photosensitizer. *J. Am. Chem. Soc.* **2014**, *136*, 8438–8449. [CrossRef]
19. Shi, H.; Guo, H.; Wang, S.; Zhang, G.; Hu, Y.; Jiang, W.; Liu, G. Visible Light Photoanode Material for Photoelectrochemical Water Splitting: A Review of Bismuth Vanadate. *Energy Fuels* **2022**, *36*, 11404–11427. [CrossRef]
20. Yang, W.; Moon, J. Recent Advances in Earth-Abundant Photocathodes for Photoelectrochemical Water Splitting. *ChemSusChem* **2019**, *12*, 1889–1899. [CrossRef]
21. Toe, C.Y.; Zhou, S.; Gunawan, M.; Lu, X.; Ng, Y.H.; Amal, R. Recent Advances and the Design Criteria of Metal Sulfide Photocathodes and Photoanodes for Photoelectrocatalysis. *J. Mater. Chem. A* **2021**, *9*, 20277–20319. [CrossRef]
22. Li, X.; Yu, J.; Low, J.; Fang, Y.; Xiao, J.; Chen, X. Engineering Heterogeneous Semiconductors for Solar Water Splitting. *J. Mater. Chem. A* **2015**, *3*, 2485–2534. [CrossRef]
23. Chen, Q.; Fan, G.; Fu, H.; Li, Z.; Zou, Z. Tandem Photoelectrochemical Cells for Solar Water Splitting. *Adv. Phys. X* **2018**, *3*, 1487267. [CrossRef]
24. Prévot, M.S.; Sivula, K. Photoelectrochemical Tandem Cells for Solar Water Splitting. *J. Phys. Chem. C* **2013**, *117*, 17879–17893. [CrossRef]
25. Chen, Z.; Jaramillo, T.F.; Deutsch, T.G.; Kleiman-Shwarsctein, A.; Forman, A.J.; Gaillard, N.; Garland, R.; Takanabe, K.; Heske, C.; Sunkara, M.; et al. Accelerating Materials Development for Photoelectrochemical Hydrogen Production: Standards for Methods, Definitions, and Reporting Protocols. *J. Mater. Res.* **2010**, *25*, 3–16. [CrossRef]

26. Lin, Y.; Battaglia, C.; Boccard, M.; Hettick, M.; Yu, Z.; Ballif, C.; Ager, J.W.; Javey, A. Amorphous Si Thin Film Based Photocathodes with High Photovoltage for Efficient Hydrogen Production. *Nano Lett.* **2013**, *13*, 5615–5618. [CrossRef]
27. Lee, M.H.; Takei, K.; Zhang, J.; Kapadia, R.; Zheng, M.; Chen, Y.-Z.; Nah, J.; Matthews, T.S.; Chueh, Y.-L.; Ager, J.W.; et al. P-Type InP Nanopillar Photocathodes for Efficient Solar-Driven Hydrogen Production. *Angew. Chem. Int. Ed.* **2012**, *51*, 10760–10764. [CrossRef]
28. Liu, C.; Sun, J.; Tang, J.; Yang, P. Zn-Doped p-Type Gallium Phosphide Nanowire Photocathodes from a Surfactant-Free Solution Synthesis. *Nano Lett.* **2012**, *12*, 5407–5411. [CrossRef]
29. Yang, W.; Kim, J.H.; Hutter, O.S.; Phillips, L.J.; Tan, J.; Park, J.; Lee, H.; Major, J.D.; Lee, J.S.; Moon, J. Benchmark Performance of Low-Cost Sb_2Se_3 Photocathodes for Unassisted Solar Overall Water Splitting. *Nat. Commun.* **2020**, *11*, 861. [CrossRef]
30. Meena, B.; Kumar, M.; Gupta, S.; Sinha, L.; Subramanyam, P.; Subrahmanyam, C. Rational Design of TiO2/BiSbS3 Heterojunction for Efficient Solar Water Splitting. *Sustain. Energy Technol. Assessments* **2022**, *49*, 101775. [CrossRef]
31. Li, C.; He, J.; Xiao, Y.; Li, Y.; Delaunay, J.-J. Earth-Abundant Cu-Based Metal Oxide Photocathodes for Photoelectrochemical Water Splitting. *Energy Environ. Sci.* **2020**, *13*, 3269–3306. [CrossRef]
32. Paracchino, A.; Laporte, V.; Sivula, K.; Grätzel, M.; Thimsen, E. Highly Active Oxide Photocathode for Photoelectrochemical Water Reduction. *Nat. Mater.* **2011**, *10*, 456–461. [CrossRef] [PubMed]
33. Hara, M. Cu_2O as a Photocatalyst for Overall Water Splitting under Visible Light Irradiation. *Chem. Commun.* **1998**, *2*, 357–358. [CrossRef]
34. Ding, C.; Shi, J.; Wang, Z.; Li, C. Photoelectrocatalytic Water Splitting: Significance of Cocatalysts, Electrolyte, and Interfaces. *ACS Catal.* **2017**, *7*, 675–688. [CrossRef]
35. Luo, J.; Steier, L.; Son, M.-K.; Schreier, M.; Mayer, M.T.; Grätzel, M. Cu_2O Nanowire Photocathodes for Efficient and Durable Solar Water Splitting. *Nano Lett.* **2016**, *16*, 1848–1857. [CrossRef]
36. Son, M.-K.; Pan, L.; Mayer, M.T.; Hagfeldt, A.; Grätzel, M.; Luo, J. Structural and Compositional Investigations on the Stability of Cuprous Oxide Nanowire Photocathodes for Photoelectrochemical Water Splitting. *ACS Appl. Mater. Interfaces* **2021**, *13*, 55080–55091. [CrossRef]
37. Zhao, Y.; Song, W.; Wang, D.; Chen, H.; Zhou, G. Enhanced Light Trapping and Charge Separation via Pyramidal Cu_2O/NiCo-LDH Photocathode for Efficient Water Splitting. *ACS Appl. Energy Mater.* **2022**, *5*, 992–1001. [CrossRef]
38. Dubale, A.A.; Tamirat, A.G.; Chen, H.-M.; Berhe, T.A.; Pan, C.-J.; Su, W.-N.; Hwang, B.-J. A Highly Stable CuS and CuS–Pt Modified Cu_2O/CuO Heterostructure as an Efficient Photocathode for the Hydrogen Evolution Reaction. *J. Mater. Chem. A* **2016**, *4*, 2205–2216. [CrossRef]
39. Son, M.K.; Steier, L.; Schreier, M.; Mayer, M.T.; Luo, J.; Grätzel, M. A Copper Nickel Mixed Oxide Hole Selective Layer for Au-Free Transparent Cuprous Oxide Photocathodes. *Energy Environ. Sci.* **2017**, *10*, 912–918. [CrossRef]
40. Subramanyam, P.; Meena, B.; Biju, V.; Misawa, H.; Challapalli, S. Emerging Materials for Plasmon-Assisted Photoelectrochemical Water Splitting. *J. Photochem. Photobiol. C Photochem. Rev.* **2022**, *51*, 100472. [CrossRef]
41. Lin, Y.-C.; Hsu, L.-C.; Lin, C.-Y.; Chiang, C.-L.; Chou, C.-M.; Wu, W.-W.; Chen, S.-Y.; Lin, Y.-G. Sandwich-Nanostructured n-Cu_2O/AuAg/p-Cu_2O Photocathode with Highly Positive Onset Potential for Improved Water Reduction. *ACS Appl. Mater. Interfaces* **2019**, *11*, 38625–38632. [CrossRef] [PubMed]
42. Kumar, M.; Ghosh, C.C.; Meena, B.; Ma, T.; Subrahmanyam, C. Plasmonic Au Nanoparticle Sandwiched $CuBi_2O_4/S_2S_3$ Photocathode with Multi-Mediated Electron Transfer for Efficient Solar Water Splitting. *Sustain. Energy Fuels* **2022**, *6*, 3961–3974. [CrossRef]
43. Septina, W.; Prabhakar, R.R.; Wick, R.; Moehl, T.; Tilley, S.D. Stabilized Solar Hydrogen Production with CuO/CdS Heterojunction Thin Film Photocathodes. *Chem. Mater.* **2017**, *29*, 1735–1743. [CrossRef]
44. Masudy-Panah, S.; Moakhar, R.S.; Chua, C.S.; Tan, H.R.; Wong, T.I.; Chi, D.; Dalapati, G.K. Nanocrystal Engineering of Sputter-Grown CuO Photocathode for Visible-Light-Driven Electrochemical Water Splitting. *ACS Appl. Mater. Interfaces* **2016**, *8*, 1206–1213. [CrossRef] [PubMed]
45. Cots, A.; Bonete, P.; Gómez, R. Improving the Stability and Efficiency of CuO Photocathodes for Solar Hydrogen Production through Modification with Iron. *ACS Appl. Mater. Interfaces* **2018**, *10*, 26348–26356. [CrossRef] [PubMed]
46. Wang, Z.; Zhang, L.; Schülli, T.U.; Bai, Y.; Monny, S.A.; Du, A.; Wang, L. Identifying Copper Vacancies and Their Role in the CuO Based Photocathode for Water Splitting. *Angew. Chem.* **2019**, *131*, 17768–17773. [CrossRef]
47. Nakabayashi, Y.; Nishikawa, M.; Nosaka, Y. Fabrication of $CuBi_2O_4$ Photocathode through Novel Anodic Electrodeposition for Solar Hydrogen Production. *Electrochim. Acta* **2014**, *125*, 191–198. [CrossRef]
48. Park, S.; Baek, J.H.; Zhang, L.; Lee, J.M.; Stone, K.H.; Cho, I.S.; Guo, J.; Jung, H.S.; Zheng, X. Rapid Flame-Annealed $CuFe_2O_4$ as Efficient Photocathode for Photoelectrochemical Hydrogen Production. *ACS Sustain. Chem. Eng.* **2019**, *7*, 5867–5874. [CrossRef]
49. Tan, R.; Hwang, S.W.; Sivanantham, A.; Cho, I.S. Solution Synthesis and Activation of Spinel $CuAl_2O_4$ Film for Solar Water-Splitting. *J. Catal.* **2021**, *400*, 218–227. [CrossRef]
50. Crespo, C.T. CuNbO3 as a Solar Energy Converter to Fuel and Electricity. *Sol. Energy Mater. Sol. Cells* **2018**, *179*, 305–311. [CrossRef]
51. Creissen, C.E.; Warnan, J.; Reisner, E. Solar H_2 Generation in Water with a $CuCrO_2$ Photocathode Modified with an Organic Dye and Molecular Ni Catalyst. *Chem. Sci.* **2018**, *9*, 1439–1447. [CrossRef] [PubMed]

52. Monny, S.A.; Zhang, L.; Wang, Z.; Luo, B.; Konarova, M.; Du, A.; Wang, L. Fabricating Highly Efficient Heterostructured $CuBi_2O_4$ Photocathodes for Unbiased Water Splitting. *J. Mater. Chem. A* **2020**, *8*, 2498–2504. [CrossRef]
53. Kang, D.; Hill, J.C.; Park, Y.; Choi, K.-S. Photoelectrochemical Properties and Photostabilities of High Surface Area $CuBi_2O_4$ and Ag-Doped $CuBi_2O_4$ Photocathodes. *Chem. Mater.* **2016**, *28*, 4331–4340. [CrossRef]
54. Xu, N.; Li, F.; Gao, L.; Hu, H.; Hu, Y.; Long, X.; Ma, J.; Jin, J. N,Cu-Codoped Carbon Nanosheet/Au/$CuBi_2O_4$ Photocathodes for Efficient Photoelectrochemical Water Splitting. *ACS Sustain. Chem. Eng.* **2018**, *6*, 7257–7264. [CrossRef]
55. Kim, J.H.; Kim, H.E.; Kim, J.H.; Lee, J.S. Ferrites: Emerging Light Absorbers for Solar Water Splitting. *J. Mater. Chem. A* **2020**, *8*, 9447–9482. [CrossRef]
56. Maitra, S.; Pal, S.; Maitra, T.; Halder, S.; Roy, S. Solvothermal Etching-Assisted Phase and Morphology Tailoring in Highly Porous $CuFe_2O_4$ Nanoflake Photocathodes for Solar Water Splitting. *Energy Fuels* **2021**, *35*, 14087–14100. [CrossRef]
57. Atacan, K.; Topaloğlu, B.; Özacar, M. New CuFe2O4/Amorphous Manganese Oxide Nanocomposites Used as Photocatalysts in Photoelectrochemical Water Splitting. *Appl. Catal. A Gen.* **2018**, *564*, 33–42. [CrossRef]
58. Oh, Y.; Yang, W.; Kim, J.; Jeong, S.; Moon, J. Enhanced Photocurrent of Transparent $CuFeO_2$ Photocathodes by Self-Light-Harvesting Architecture. *ACS Appl. Mater. Interfaces* **2017**, *9*, 14078–14087. [CrossRef]
59. Siripala, W.; Ivanovskaya, A.; Jaramillo, T.F.; Baeck, S.H.; McFarland, E.W. A Cu_2O/TiO_2 Heterojunction Thin Film Cathode for Photoelectrocatalysis. *Sol. Energy Mater. Sol. Cells* **2003**, *77*, 229–237. [CrossRef]
60. Zhang, Z.; Dua, R.; Zhang, L.; Zhu, H.; Zhang, H.; Wang, P. Carbon-Layer-Protected Cuprous Oxide Nanowire Arrays for Efficient Water Reduction. *ACS Nano* **2013**, *7*, 1709–1717. [CrossRef]
61. Paracchino, A.; Mathews, N.; Hisatomi, T.; Stefik, M.; Tilley, S.D.; Grätzel, M. Ultrathin Films on Copper(i) Oxide Water Splitting Photocathodes: A Study on Performance and Stability. *Energy Environ. Sci.* **2012**, *5*, 8673. [CrossRef]
62. Tilley, S.D.; Schreier, M.; Azevedo, J.; Stefik, M.; Graetzel, M. Ruthenium Oxide Hydrogen Evolution Catalysis on Composite Cuprous Oxide Water-Splitting Photocathodes. *Adv. Funct. Mater.* **2014**, *24*, 303–311. [CrossRef]
63. Azevedo, J.; Steier, L.; Dias, P.; Stefik, M.; Sousa, C.T.; Araújo, J.P.; Mendes, A.; Graetzel, M.; Tilley, S.D. On the Stability Enhancement of Cuprous Oxide Water Splitting Photocathodes by Low Temperature Steam Annealing. *Energy Environ. Sci.* **2014**, *7*, 4044–4052. [CrossRef]
64. Morales-Guio, C.G.; Tilley, S.D.; Vrubel, H.; Grätzel, M.; Hu, X. Hydrogen Evolution from a Copper(I) Oxide Photocathode Coated with an Amorphous Molybdenum Sulphide Catalyst. *Nat. Commun.* **2014**, *5*, 3059. [CrossRef]
65. Morales-Guio, C.G.; Liardet, L.; Mayer, M.T.; Tilley, S.D.; Grätzel, M.; Hu, X. Photoelectrochemical Hydrogen Production in Alkaline Solutions Using Cu_2O Coated with Earth-Abundant Hydrogen Evolution Catalysts. *Angew. Chem. Int. Ed.* **2014**, *54*, 664–667. [CrossRef]
66. Chen, D.; Liu, Z.; Guo, Z.; Yan, W.; Ruan, M. Decorating Cu_2O Photocathode with Noble-Metal-Free Al and NiS Cocatalysts for Efficient Photoelectrochemical Water Splitting by Light Harvesting Management and Charge Separation Design. *Chem. Eng. J.* **2020**, *381*, 122655. [CrossRef]
67. Kim, J.S.; Cho, S.W.; Deshpande, N.G.; Kim, Y.B.; Yun, Y.D.; Jung, S.H.; Kim, D.S.; Cho, H.K. Toward Robust Photoelectrochemical Operation of Cuprous Oxide Nanowire Photocathodes Using a Strategically Designed Solution-Processed Titanium Oxide Passivation Coating. *ACS Appl. Mater. Interfaces* **2019**, *11*, 14840–14847. [CrossRef]
68. Zhou, M.; Guo, Z.; Liu, Z. FeOOH as Hole Transfer Layer to Retard the Photocorrosion of Cu_2O for Enhanced Photoelctrochemical Performance. *Appl. Catal. B Environ.* **2020**, *260*, 118213. [CrossRef]
69. Pan, L.; Liu, Y.; Yao, L.; Ren, D.; Sivula, K.; Grätzel, M.; Hagfeldt, A. Cu_2O Photocathodes with Band-Tail States Assisted Hole Transport for Standalone Solar Water Splitting. *Nat. Commun.* **2020**, *11*, 318. [CrossRef]
70. Fu, X.; Chang, H.; Shang, Z.; Liu, P.; Liu, J.; Luo, H. Three-Dimensional Cu_2O Nanorods Modified by Hydrogen Treated $Ti_3C_2T_X$ MXene with Enriched Oxygen Vacancies as a Photocathode and a Tandem Cell for Unassisted Solar Water Splitting. *Chem. Eng. J.* **2020**, *381*, 122001. [CrossRef]
71. Tawfik, W.Z.; Hassan, M.A.; Johar, M.A.; Ryu, S.-W.; Lee, J.K. Highly Conversion Efficiency of Solar Water Splitting over P-Cu_2O/ZnO Photocatalyst Grown on a Metallic Substrate. *J. Catal.* **2019**, *374*, 276–283. [CrossRef]
72. Caretti, M.; Lazouni, L.; Xia, M.; Wells, R.A.; Nussbaum, S.; Ren, D.; Grätzel, M.; Sivula, K. Transparency and Morphology Control of Cu_2O Photocathodes via an in Situ Electroconversion. *ACS Energy Lett.* **2022**, *7*, 1618–1625. [CrossRef]
73. Varunkumar, K.; Sellappan, R. Photoelectrochemical Behaviour of $CuBi_2O_4$@MoS_2 Photocathode for Solar Water Splitting. *Mater. Chem. Phys.* **2021**, *261*, 124245. [CrossRef]
74. Wang, F.; Chemseddine, A.; Abdi, F.F.; van de Krol, R.; Berglund, S.P. Spray Pyrolysis of $CuBi_2O_4$ Photocathodes: Improved Solution Chemistry for Highly Homogeneous Thin Films. *J. Mater. Chem. A* **2017**, *5*, 12838–12847. [CrossRef]
75. Berglund, S.P.; Abdi, F.F.; Bogdanoff, P.; Chemseddine, A.; Friedrich, D.; van de Krol, R. Comprehensive Evaluation of $CuBi_2O_4$ as a Photocathode Material for Photoelectrochemical Water Splitting. *Chem. Mater.* **2016**, *28*, 4231–4242. [CrossRef]
76. Park, H.S.; Lee, C.Y.; Reisner, E. Photoelectrochemical Reduction of Aqueous Protons with a CuO|$CuBi_2O_4$ Heterojunction under Visible Light Irradiation. *Phys. Chem. Chem. Phys.* **2014**, *16*, 22462–22465. [CrossRef]
77. Lee, J.; Yoon, H.; Choi, K.S.; Kim, S.; Seo, S.; Song, J.; Choi, B.; Ryu, J.; Ryu, S.; Oh, J.; et al. Template Engineering of CuBi2O4 Single-Crystal Thin Film Photocathodes. *Small* **2020**, *16*, 2002429. [CrossRef]

78. Lee, J.; Yoon, H.; Kim, S.; Seo, S.; Song, J.; Choi, B.-U.; Choi, S.Y.; Park, H.; Ryu, S.; Oh, J.; et al. Long-Term Stabilized High-Density $CuBi_2O_4$/NiO Heterostructure Thin Film Photocathode Grown by Pulsed Laser Deposition. *Chem. Commun.* **2019**, *55*, 12447–12450. [CrossRef]
79. Wei, S.; Xu, N.; Li, F.; Long, X.; Hu, Y.; Gao, L.; Wang, C.; Li, S.; Ma, J.; Jin, J. Rationally Designed Heterojunction on a $CuBi_2O_4$ Photocathode for Improved Activity and Stability during Photoelectrochemical Water Reduction. *ChemElectroChem* **2019**, *6*, 3367–3374. [CrossRef]
80. Wei, S.; Wang, C.; Long, X.; Wang, T.; Wang, P.; Zhang, M.; Li, S.; Ma, J.; Jin, J.; Wu, L. A Oxygen Vacancy-Modulated Homojunction Structural $CuBi_2O_4$ photocathodes for Efficient Solar Water Reduction. *Nanoscale* **2020**, *12*, 15193–15200. [CrossRef]
81. Cao, D.; Nasori, N.; Wang, Z.; Mi, Y.; Wen, L.; Yang, Y.; Qu, S.; Wang, Z.; Lei, Y. P-Type $CuBi_2O_4$: An Easily Accessible Photocathodic Material for High-Efficiency Water Splitting. *J. Mater. Chem. A* **2016**, *4*, 8995–9001. [CrossRef]
82. Pulipaka, S.; Boni, N.; Ummethala, G.; Meduri, P. CuO/$CuBi_2O_4$ Heterojunction Photocathode: High Stability and Current Densities for Solar Water Splitting. *J. Catal.* **2020**, *387*, 17–27. [CrossRef]
83. Wang, F.; Septina, W.; Chemseddine, A.; Abdi, F.F.; Friedrich, D.; Bogdanoff, P.; van de Krol, R.; Tilley, S.D.; Berglund, S.P. Gradient Self-Doped $CuBi_2O_4$ with Highly Improved Charge Separation Efficiency. *J. Am. Chem. Soc.* **2017**, *139*, 15094–15103. [CrossRef] [PubMed]
84. Prévot, M.S.; Guijarro, N.; Sivula, K. Enhancing the Performance of a Robust Sol-Gel-Processed p-Type Delafossite $CuFeO_2$ Photocathode for Solar Water Reduction. *ChemSusChem* **2015**, *8*, 1359–1367. [CrossRef] [PubMed]
85. Jang, Y.J.; Park, Y.B.; Kim, H.E.; Choi, Y.H.; Choi, S.H.; Lee, J.S. Oxygen-Intercalated $CuFeO_2$ Photocathode Fabricated by Hybrid Microwave Annealing for Efficient Solar Hydrogen Production. *Chem. Mater.* **2016**, *28*, 6054–6061. [CrossRef]
86. Prévot, M.S.; Li, Y.; Guijarro, N.; Sivula, K. Improving Charge Collection with Delafossite Photocathodes: A Host–Guest $CuAlO_2$/$CuFeO_2$ Approach. *J. Mater. Chem. A* **2016**, *4*, 3018–3026. [CrossRef]
87. Li, M.; Zhao, R.; Su, Y.; Yang, Z.; Zhang, Y. Carbon Quantum Dots Decorated Cu_2S Nanowire Arrays for Enhanced Photoelectrochemical Performance. *Nanoscale* **2016**, *8*, 8559–8567. [CrossRef]
88. Chen, L.; Hu, H.; Chen, Y.; Gao, J.; Li, G. Plasmonic Cu_2-XS Nanoparticles: A Brief Introduction of Optical Properties and Applications. *Mater. Adv.* **2021**, *2*, 907–926. [CrossRef]
89. Yu, Y.-X.; Pan, L.; Son, M.-K.; Mayer, M.T.; Zhang, W.-D.; Hagfeldt, A.; Luo, J.; Grätzel, M. Solution-Processed Cu_2S Photocathodes for Photoelectrochemical Water Splitting. *ACS Energy Lett.* **2018**, *3*, 760–766. [CrossRef]
90. Liu, Z.; Lu, X.; Chen, D. Photoelectrochemical Water Splitting of $CuInS_2$ Photocathode Collaborative Modified with Separated Catalysts Based on Efficient Photogenerated Electron–Hole Separation. *ACS Sustain. Chem. Eng.* **2018**, *6*, 10289–10294. [CrossRef]
91. Feng, X.; Li, R.; Wang, M.; Chen, Y. Switchable Synthesis of P- and n-Type Cu–In–S Grooved Pyramid-like Microcrystals for Unassisted Photoelectrochemical Water Splitting. *J. Mater. Chem. A* **2018**, *6*, 11180–11188. [CrossRef]
92. Liu, Z.; Zhou, M. Co-Modification with Cost-Effective Nickel Oxides and Nickel Sulfides on $CuInS_2$ Nanosheets Photocathode for Enhanced Photoelectrochemical Performance. *ACS Sustain. Chem. Eng.* **2020**, *8*, 512–519. [CrossRef]
93. Gunawan; Septina, W.; Harada, T.; Nose, Y.; Ikeda, S. Investigation of the Electric Structures of Heterointerfaces in Pt- and In_2S_3 -Modified $CuInS_2$ Photocathodes Used for Sunlight-Induced Hydrogen Evolution. *ACS Appl. Mater. Interfaces* **2015**, *7*, 16086–16092. [CrossRef] [PubMed]
94. Chae, S.Y.; Kim, Y.; Park, E.D.; Im, S.H.; Joo, O.-S. $CuInS_2$ Photocathodes with Atomic Gradation-Controlled (Ta,Mo) x (O,S) y Passivation Layers for Efficient Photoelectrochemical H_2 Production. *ACS Appl. Mater. Interfaces* **2021**, *13*, 58447–58457. [CrossRef] [PubMed]
95. Connor, S.T.; Weil, B.D.; Misra, S.; Cui, Y.; Toney, M.F. Behaviors of Fe, Zn, and Ga Substitution in $CuInS_2$ Nanoparticles Probed with Anomalous X-Ray Diffraction. *Chem. Mater.* **2013**, *25*, 320–325. [CrossRef]
96. Vahidshad, Y.; Tahir, M.N.; Zad, A.I.; Mirkazemi, S.M.; Ghasemzadeh, R.; Huesmann, H.; Tremel, W. Structural and Optical Study of Ga^{3+} Substitution in $CuInS_2$ Nanoparticles Synthesized by a One-Pot Facile Method. *J. Phys. Chem. C* **2014**, *118*, 24670–24679. [CrossRef]
97. Septina, W.; Gunawan; Ikeda, S.; Harada, T.; Higashi, M.; Abe, R.; Matsumura, M. Photosplitting of Water from Wide-Gap $Cu(In,Ga)S_2$ Thin Films Modified with a CdS Layer and Pt Nanoparticles for a High-Onset-Potential Photocathode. *J. Phys. Chem. C* **2015**, *119*, 8576–8583. [CrossRef]
98. Kaga, H.; Tsutsui, Y.; Nagane, A.; Iwase, A.; Kudo, A. An Effect of Ag(i)-Substitution at Cu Sites in $CuGaS_2$ on Photocatalytic and Photoelectrochemical Properties for Solar Hydrogen Evolution. *J. Mater. Chem. A* **2015**, *3*, 21815–21823. [CrossRef]
99. Teimouri, R.; Mohammadpour, R. Potential Application of $CuSbS_2$ as the Hole Transport Material in Perovskite Solar Cell: A Simulation Study. *Superlattices Microstruct.* **2018**, *118*, 116–122. [CrossRef]
100. Ramasamy, K.; Tien, B.; Archana, P.S.; Gupta, A. Copper Antimony Sulfide ($CuSbS_2$) Mesocrystals: A Potential Counter Electrode Material for Dye-Sensitized Solar Cells. *Mater. Lett.* **2014**, *124*, 227–230. [CrossRef]
101. Macías, C.; Lugo, S.; Benítez, Á.; López, I.; Kharissov, B.; Vázquez, A.; Peña, Y. Thin Film Solar Cell Based on $CuSbS_2$ Absorber Prepared by Chemical Bath Deposition (CBD). *Mater. Res. Bull.* **2017**, *87*, 161–166. [CrossRef]
102. Medina-Montes, M.I.; Campos-González, E.; Morales-Luna, M.; Sánchez, T.G.; Becerril-Silva, M.; Mayén-Hernández, S.A.; de Moure-Flores, F.; Santos-Cruz, J. Development of Phase-Pure $CuSbS_2$ Thin Films by Annealing Thermally Evaporated CuS/Sb_2S_3 Stacking Layer for Solar Cell Applications. *Mater. Sci. Semicond. Process.* **2018**, *80*, 74–84. [CrossRef]

103. Rastogi, A.C.; Janardhana, N.R. Properties of $CuSbS_2$ Thin Films Electrodeposited from Ionic Liquids as P-Type Absorber for Photovoltaic Solar Cells. *Thin Solid Films* **2014**, *565*, 285–292. [CrossRef]
104. Wang, L.; Zhao, X.; Yang, Z.; Ng, B.K.; Jiang, L.; Lai, Y.; Jia, M. $CuSbS_2$ Solar Cells Using CdS, In_2S_3 and the In/Cd-Based Hybrid Buffers. *J. Electron. Mater.* **2021**, *50*, 3283–3287. [CrossRef]
105. Aquino, J.A.R.; Vela, D.L.R.; Shaji, S.; Avellaneda, D.A.; Krishnan, B. Spray Pyrolysed Thin Films of Copper Antimony Sulfide as Photovoltaic Absorber. *Phys. Status Solidi C* **2016**, *13*, 24–29. [CrossRef]
106. Zhang, L.; Li, Y.; Li, X.; Li, C.; Zhang, R.; Delaunay, J.-J.; Zhu, H. Solution-Processed $CuSbS_2$ Thin Film: A Promising Earth-Abundant Photocathode for Efficient Visible-Light-Driven Hydrogen Evolution. *Nano Energy* **2016**, *28*, 135–142. [CrossRef]
107. Kumar, M.; Dubey, A.; Adhikari, N.; Venkatesan, S.; Qiao, Q. Strategic Review of Secondary Phases, Defects and Defect-Complexes in Kesterite CZTS-Se Solar Cells. *Energy Environ. Sci.* **2015**, *8*, 3134–3159. [CrossRef]
108. Rovelli, L.; Tilley, S.D.; Sivula, K. Optimization and Stabilization of Electrodeposited Cu_2ZnSnS_4 Photocathodes for Solar Water Reduction. *ACS Appl. Mater. Interfaces* **2013**, *5*, 8018–8024. [CrossRef]
109. Jiang, F.; Gunawan; Harada, T.; Kuang, Y.; Minegishi, T.; Domen, K.; Ikeda, S. Pt/In_2S_3/CdS/Cu_2ZnSnS_4 Thin Film as an Efficient and Stable Photocathode for Water Reduction under Sunlight Radiation. *J. Am. Chem. Soc.* **2015**, *137*, 13691–13697. [CrossRef]
110. Huang, D.; Wang, K.; Yu, L.; Nguyen, T.H.; Ikeda, S.; Jiang, F. Over 1% Efficient Unbiased Stable Solar Water Splitting Based on a Sprayed Cu_2ZnSnS_4 Photocathode Protected by a HfO_2 Photocorrosion-Resistant Film. *ACS Energy Lett.* **2018**, *3*, 1875–1881. [CrossRef]
111. Yang, W.; Oh, Y.; Kim, J.; Jeong, M.J.; Park, J.H.; Moon, J. Molecular Chemistry-Controlled Hybrid Ink-Derived Efficient Cu_2ZnSnS_4 Photocathodes for Photoelectrochemical Water Splitting. *ACS Energy Lett.* **2016**, *1*, 1127–1136. [CrossRef]
112. Tay, Y.F.; Kaneko, H.; Chiam, S.Y.; Lie, S.; Zheng, Q.; Wu, B.; Hadke, S.S.; Su, Z.; Bassi, P.S.; Bishop, D.; et al. Solution-Processed Cd-Substituted CZTS Photocathode for Efficient Solar Hydrogen Evolution from Neutral Water. *Joule* **2018**, *2*, 537–548. [CrossRef]
113. Tay, Y.F.; Hadke, S.S.; Zhang, M.; Lim, N.; Chiam, S.Y.; Wong, L.H. Improving the Interfacial Properties of CZTS Photocathodes by Ag Substitution. *J. Mater. Chem. A* **2020**, *8*, 8862–8867. [CrossRef]
114. Kumar, S.M.; Madhusudanan, S.P.; Rajamani, A.R.; Siaj, M.; Batabyal, S.K. Barium Substitution in Kesterite $Cu_2Zn_SnS_4$: $Cu_2Zn_{1-x}Ba_xSnS_4$ Quinary Alloy Thin Films for Efficient Solar Energy Harvesting. *Cryst. Growth Des.* **2020**, *20*, 4387–4394. [CrossRef]
115. Todorov, T.; Gunawan, O.; Guha, S. A Road towards 25% Efficiency and beyond: Perovskite Tandem Solar Cells. *Mol. Syst. Des. Eng.* **2016**, *1*, 370–376. [CrossRef]
116. Márquez, J.A.; Sun, J.-P.; Stange, H.; Ali, H.; Choubrac, L.; Schäfer, S.; Hages, C.J.; Leifer, K.; Unold, T.; Mitzi, D.B.; et al. High-Temperature Decomposition of Cu_2BaSnS_4 with Sn Loss Reveals Newly Identified Compound $Cu_2Ba_3SnS_8$. *J. Mater. Chem. A* **2020**, *8*, 11346–11353. [CrossRef]
117. Xie, J.; Yi, Q.; Zhang, F.; Bagheri, R.; Zheng, F.; Zou, G. Large-Grained Cu_2BaSnS_4 Films for Photocathodes. *ACS Appl. Mater. Interfaces* **2019**, *11*, 33102–33108. [CrossRef]
118. Ge, J.; Roland, P.J.; Koirala, P.; Meng, W.; Young, J.L.; Petersen, R.; Deutsch, T.G.; Teeter, G.; Ellingson, R.J.; Collins, R.W.; et al. Employing Overlayers To Improve the Performance of Cu_2BaSnS_4 Thin Film Based Photoelectrochemical Water Reduction Devices. *Chem. Mater.* **2017**, *29*, 916–920. [CrossRef]
119. Zhou, Y.; Shin, D.; Ngaboyamahina, E.; Han, Q.; Parker, C.B.; Mitzi, D.B.; Glass, J.T. Efficient and Stable Pt/TiO_2/CdS/$Cu_2BaSn(S,Se)_4$ Photocathode for Water Electrolysis Applications. *ACS Energy Lett.* **2018**, *3*, 177–183. [CrossRef]
120. Song, J.; Teymur, B.; Zhou, Y.; Ngaboyamahina, E.; Mitzi, D.B. Porous $Cu_2BaSn(S,Se)_4$ Film as a Photocathode Using Non-Toxic Solvent and a Ball-Milling Approach. *ACS Appl. Energy Mater.* **2021**, *4*, 81–87. [CrossRef]
121. Zhang, X.; Yang, W.; Niu, W.; Adams, P.; Siol, S.; Wang, Z.; Tilley, S.D. Thiol-Amine-Based Solution Processing of Cu_2S Thin Films for Photoelectrochemical Water Splitting. *ChemSusChem* **2021**, *14*, 3967–3974. [CrossRef] [PubMed]
122. Li, Z.; Zhang, Z. Tetrafunctional Cu2S Thin Layers on Cu2O Nanowires for Efficient Photoelectrochemical Water Splitting. *Nano Res.* **2018**, *11*, 1530–1540. [CrossRef]
123. Bai, Z.; Zhang, Y. A Cu_2O/CuS-ZnO/CdS Tandem Photoelectrochemical Cell for Self-Driven Solar Water Splitting. *J. Alloys Compd.* **2017**, *698*, 133–140. [CrossRef]
124. Zhang, W.; Chen, R.; Yin, Z.; Wang, X.; Wang, Z.; Fan, F.; Ma, Y. Surface Assistant Charge Separation in PEC Cu_2S–Ni/Cu_2O Cathode. *ACS Appl. Mater. Interfaces* **2019**, *11*, 34000–34009. [CrossRef] [PubMed]
125. Li, M.; Chen, L.; Su, Y.; Yin, H.; Hu, K. Hexagonally Ordered Microbowl Arrays Decorated with Ultrathin $CuInS_2$ Nanosheets for Enhanced Photoelectrochemical Performance. *J. Energy Chem.* **2020**, *51*, 134–142. [CrossRef]
126. Cai, Q.; Liu, Z.; Han, C.; Tong, Z.; Ma, C. $CuInS_2$/Sb_2S_3 Heterostructure Modified with Noble Metal Co-Catalyst for Efficient Photoelectrochemical Water Splitting. *J. Alloys Compd.* **2019**, *795*, 319–326. [CrossRef]
127. Li, M.; Zhao, R.; Su, Y.; Hu, J.; Yang, Z.; Zhang, Y. Synthesis of $CuInS_2$ Nanowire Arrays via Solution Transformation of Cu_2S Self-Template for Enhanced Photoelectrochemical Performance. *Appl. Catal. B Environ.* **2017**, *203*, 715–724. [CrossRef]
128. Matoba, K.; Matsuda, Y.; Takahashi, M.; Sakata, Y.; Zhang, J.; Higashimoto, S. Fabrication of Pt/In2S3/CuInS2 Thin Film as Stable Photoelectrode for Water Splitting under Solar Light Irradiation. *Catal. Today* **2021**, *375*, 87–93. [CrossRef]
129. Luo, J.; Tilley, S.D.; Steier, L.; Schreier, M.; Mayer, M.T.; Fan, H.J.; Grätzel, M. Solution Transformation of Cu_2O into $CuInS_2$ for Solar Water Splitting. *Nano Lett.* **2015**, *15*, 1395–1402. [CrossRef]

130. Yang, W.; Oh, Y.; Kim, J.; Kim, H.; Shin, H.; Moon, J. Photoelectrochemical Properties of Vertically Aligned $CuInS_2$ Nanorod Arrays Prepared via Template-Assisted Growth and Transfer. *ACS Appl. Mater. Interfaces* **2016**, *8*, 425–431. [CrossRef]
131. Zhang, F.; Chen, Y.; Zhou, W.; Ren, C.; Gao, H.; Tian, G. Hierarchical SnS_2/$CuInS_2$ Nanosheet Heterostructure Films Decorated with C_{60} for Remarkable Photoelectrochemical Water Splitting. *ACS Appl. Mater. Interfaces* **2019**, *11*, 9093–9101. [CrossRef]
132. Patra, B.K.; Khilari, S.; Pradhan, D.; Pradhan, N. Hybrid Dot–Disk Au-$CuInS_2$ Nanostructures as Active Photocathode for Efficient Evolution of Hydrogen from Water. *Chem. Mater.* **2016**, *28*, 4358–4366. [CrossRef]
133. Ran, F.; Li, P.; Yuan, X.; Zhang, J.; Zhang, D.; Chen, S. Fabrication of a Sb_2Se_3/$CuSbS_2$ Heterojunction Photocathode for Photoelectrochemical Water Splitting. *J. Phys. Chem. C* **2022**, *126*, 8581–8587. [CrossRef]
134. Yokoyama, D.; Minegishi, T.; Jimbo, K.; Hisatomi, T.; Ma, G.; Katayama, M.; Kubota, J.; Katagiri, H.; Domen, K. H_2 Evolution from Water on Modified Cu_2ZnSnS_4 Photoelectrode under Solar Light. *Appl. Phys. Express* **2010**, *3*, 101202. [CrossRef]
135. Wang, K.; Huang, D.; Yu, L.; Gu, H.; Ikeda, S.; Jiang, F. Environmentally Friendly Cu_2ZnSnS_4-Based Photocathode Modified with a ZnS Protection Layer for Efficient Solar Water Splitting. *J. Coll. Interface Sci.* **2019**, *536*, 9–16. [CrossRef]
136. Huang, D.; Wang, K.; Li, L.; Feng, K.; An, N.; Ikeda, S.; Kuang, Y.; Ng, Y.; Jiang, F. 3.17% Efficient Cu_2ZnSnS_4—$BiVO_4$ Integrated Tandem Cell for Standalone Overall Solar Water Splitting. *Energy Environ. Sci.* **2021**, *14*, 1480–1489. [CrossRef]
137. Xu, Z.; Guan, Z.; Yang, J.; Li, Q. Band Positions and Photoelectrochemical Properties of Solution-Processed Silver-Substituted Cu_2ZnSnS_4 Photocathode. *ACS Appl. Energy Mater.* **2019**, *2*, 2779–2785. [CrossRef]
138. Ikeda, S.; Nguyen, T.H.; Okamoto, R.; Remeika, M.; Abdellaoui, I.; Islam, M.M.; Harada, T.; Abe, R.; Sakurai, T. Effects of Incorporation of Ag into a Kesterite Cu_2ZnSnS_4 Thin Film on Its Photoelectrochemical Properties for Water Reduction. *Phys. Chem. Chem. Phys.* **2022**, *24*, 468–476. [CrossRef]
139. Wen, X.; Luo, W.; Guan, Z.; Huang, W.; Zou, Z. Boosting Efficiency and Stability of a Cu_2ZnSnS_4 Photocathode by Alloying Ge and Increasing Sulfur Pressure Simultaneously. *Nano Energy* **2017**, *41*, 18–26. [CrossRef]